

**DEVELOPMENT OF FIRE PROTECTION DUCT
FOR THE SAFETY-RELEVANT CIRCUITS**

LIM YOU YI

UNIVERSITI TUNKU ABDUL RAHMAN

**DEVELOPMENT OF FIRE PROTECTION DUCT
FOR THE SAFETY-RELEVANT CIRCUITS**

LIM YOU YI

**A project report submitted in partial fulfilment of the
requirements for the award of Bachelor of Mechanical
Engineering with Honours**

**Lee Kong Chian Faculty of Engineering and Science
Universiti Tunku Abdul Rahman**

May 2023

DECLARATION

I hereby declare that this project report is based on my original work except for citations and quotations which have been duly acknowledged. I also declare that it has not been previously and concurrently submitted for any other degree or award at UTAR or other institutions.

Signature :



Name : Lim You Yi

ID No. : 1804285

Date : 23rd April 2023

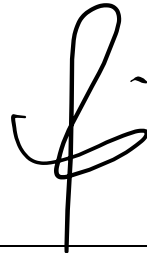
APPROVAL FOR SUBMISSION

I certify that this project report entitled **“DEVELOPMENT OF FIRE PROTECTION DUCT FOR THE SAFETY-RELEVANT CIRCUITS”** was prepared by **LIM YOU YI** has met the required standard for submission in partial fulfilment of the requirements for the award of Bachelor of Mechanical Engineering with Honours at Universiti Tunku Abdul Rahman.

Approved by,

Signature

:



Supervisor

:

Ir Ts Dr Yew Ming Chian

Date

:

28th April 2023

The copyright of this report belongs to the author under the terms of the copyright Act 1987 as qualified by Intellectual Property Policy of Universiti Tunku Abdul Rahman. Due acknowledgement shall always be made of the use of any material contained in, or derived from, this report.

© 2023, Lim You Yi. All right reserved.

ACKNOWLEDGEMENTS

I would like to thank everyone who contributed to the successful completion of this project. I would like to express my gratitude to my research supervisor, Ir. Ts. Dr. Yew Ming Chian, for his invaluable advice, guidance and enormous patience throughout the development of the research.

Next, I would like to thank all the lab staffs from levels 5 and 7 who helped me conduct the scanning electron microscopic (SEM) analysis, energy-disperse X-ray (EDX) spectroscopy test, thermogravimetric analysis (TGA) test, and Fourier-transform infrared (FTIR) spectroscopy test.

Other than that, I am also grateful for the kindness of the KBS03 Mechanical Workshop's lab staff, who have always given me some patience and guidance when I am running some physical tests in the workshop. In addition, Dr. Ting Chen Hunt also gave some recommendations when I was preparing the test samples.

Last but not least, I am appreciative of my family members who provide ongoing physical and mental support.

ABSTRACT

Fire protection ducts store and protect electrical cables during a fire outbreak. The cables provide power supplies to the active fire protective system (e.g., water sprinklers, fire alarms) and extend the time for evacuation. Fire protection duct can be fabricated by combining and assembling fire-retardant boards. The project scope focuses on formulating the water-based intumescent binder (W-IB) as the fundamental of the fire-retardant board. W-IB was proven to have better properties than the commercial magnesium oxide (MgO) board, especially in fire resistivity. The commercial MgO board possesses a low resistivity to fire and water and is not able to provide long-term protection of the underlying substrate from a high temperature and moisture environment. In the analysis, four groups of W-IB were formulated and analysed through fire resistance testing (e.g., Bunsen burner test), chemical testing (e.g., static immersion test), mechanical testing (e.g., adhesion strength test), thermal testing (e.g., TGA test), and physical testing (e.g., SEM/EDX test, FTIR test). Next, W-IB and vermiculite were combined to make fire-retardant board prototypes. To ascertain the compositions' best performance, a half-hour small-scale fire, a density measurement, a sound insulation, and a three-point flexural tests were conducted. The leading-performing fire-retardant board was then cast using the best-performing compositions. The capabilities of the fire-retardant board and the commercial MgO board were compared using a 1-hour small-scale fire test and density measurement test. The leading-performing fire-retardant board was then used to construct a small-scale fire protection duct. The results of all the tests revealed that, both pre and post of the 1-hour small-scale fire test, fire-retardant board prototype 4 (P4) has a lower weight loss percentage than commercial MgO board. Prototype P4 has a weight loss of 20.6 % lower than commercial MgO board. Thus, prototype P4 has better suitability to construct fire protection duct. On the other hand, prototype P4 also showed a lower temperature profile (100 °C) than the commercial MgO board (220 °C) when conducting the 1-hour small-scale fire test. Therefore, prototype P4 possesses an effective W-IB that can resist the fire propagation and remain its technical integrity after a 1-hour small-scale fire test.

TABLE OF CONTENTS

DECLARATION		i
APPROVAL FOR SUBMISSION		ii
ACKNOWLEDGEMENTS		iv
ABSTRACT		v
TABLE OF CONTENTS		vi
LIST OF TABLES		x
LIST OF FIGURES		xi
LIST OF SYMBOLS / ABBREVIATIONS		xiii
LIST OF APPENDICES		xv
CHAPTER		
1	INTRODUCTION	1
1.1	General Introduction	1
1.2	Importance of the Study	3
1.3	Problem Statement	4
1.4	Aim and Objectives	5
1.5	Scope and Limitation of the Study	6
1.6	Contribution of the Study	7
1.7	Outline of the Report	7
2	LITERATURE REVIEW	9
2.1	Introduction	9
2.2	Flame-retardant Fillers	9
2.2.1	Chicken Eggshell Powder	9
2.2.2	Magnesium Hydroxide	10
2.2.3	Titanium Dioxide	11
2.2.4	Calcium Carbonate	12
2.2.5	Calcium Silicate	12

	2.2.6 Aluminium Oxide	13
2.3	Flame-retardant Materials - Vermiculite	13
2.4	Binder	14
	2.4.1 Vinyl Acetate Copolymer (VAC)	14
	2.4.2 Acrylic Emulsion Copolymer	14
2.5	Flame Retardant Additives	14
	2.5.1 Ammonium Polyphosphate (APP)	15
	2.5.2 Pentaerythritol (PER)	16
	2.5.3 Melamine (MEL)	16
	2.5.4 Expandable Graphite (EG)	16
2.6	Summary	17
3	METHODOLOGY AND WORK PLAN	18
3.1	Introduction	18
3.2	Process Flowchart	19
3.3	Materials Preparation	20
3.4	Sample and Prototype Preparation	22
3.5	Testing Methods for Water-based Intumescent binder	26
	3.5.1 Bunsen Burner Test	26
	3.5.2 Static Immersion Test	27
	3.5.3 Adhesion Strength Test	28
	3.5.4 Scanning Electron Microscopy (SEM) Analysis	29
	3.5.5 Energy-disperse X-ray (EDX) Spectroscopy Test	29
	3.5.6 Thermogravimetric Analysis (TGA) Test	30
	3.5.7 Fourier-transform Infrared (FTIR) Spectroscopy Test	30
3.6	Testing Methods for Prototypes	30
	3.6.1 Half-hour Small-scale Fire Test	30
	3.6.2 Density Measurement Test	31
	3.6.3 Sound Insulation Test	31
	3.6.4 Three-point Flexural Test	33

3.7	Testing Methods for Best-Performing Fire-Retardant Board	34
3.7.1	1-hour Small-scale Fire Test	34
3.7.2	Density Measurement Test	34
3.8	Testing Methods for Fire Protection Duct	35
3.8.1	1-hour Small-scale Fire Test	35
3.9	Summary	35
4	RESULTS AND DISCUSSION	36
4.1	Introduction	36
4.2	Sample Characterization of Water-based Intumescent Binder	36
4.2.1	Bunsen Burner Test	36
4.2.2	Static Immersion Test	38
4.2.3	Adhesion Strength Test	40
4.2.4	Scanning Electron Microscopy (SEM) Analysis	42
4.2.5	Energy-disperse X-ray (EDX) Spectroscopy Test	43
4.2.6	Thermogravimetric Analysis (TGA) Test	45
4.2.7	Fourier-transform Infrared (FTIR) Spectroscopy Test	46
4.3	Sample Characterization of Prototypes	48
4.3.1	Half-hour Small-scale Fire Test	48
4.3.2	Density Measurement Test	50
4.3.3	Sound Insulation Test	51
4.3.4	Three-point Flexural Test	52
4.4	Sample Characterization of Best-Performing Fire-Retardant Board	55
4.4.1	1-hour Small-scale Fire Test	55
4.4.2	Density Measurement Test	56
4.5	Sample Characterization of Fire Protection Duct	57
4.5.1	1-hour Small-scale Fire Test	57
4.6	Cost Analysis of Fire-Retardant Board	59
4.7	Summary	61

5	CONCLUSIONS AND RECOMMENDATIONS	64
5.1	Conclusions	64
5.2	Recommendations for future work	67
	REFERENCES	69
	APPENDICES	78

LIST OF TABLES

Table 3.1:	Samples' compositions.	20
Table 3.2:	Prototypes' compositions.	21
Table 4.1:	Char layer thickness and equilibrium temperature of each sample.	37
Table 4.2:	Weight Change Percentage among all the samples.	39
Table 4.3:	Density Changes of all Prototypes and the commercial MgO board.	50
Table 4.4:	The Average Sound Absorption Coefficient of the Sample Prototype.	52
Table 4.5:	Flexural Stress and Flexural Modulus of the prototypes.	54
Table 4.6:	Density changes of Prototype P4 and the commercial MgO board.	57
Table 4.7:	The Price required to cast a 0.8 kg, 175 mm x 175 mm x 30 mm Fire-retardant board.	59
Table 4.8:	Summary of the W-IB testing results.	61
Table 4.9:	Summary of the Prototypes' testing results.	62
Table 4.10:	Summary of the Best-performing Fire-retardant board testing results.	62
Table 4.11:	Summary of the Fire protection duct's testing result.	63

LIST OF FIGURES

Figure 1.1:	Fire Protective Compartment.	2
Figure 1.2:	Electrical Cable Encasement.	2
Figure 1.3:	Extraction Ductwork.	2
Figure 1.4:	Fire Protection Duct.	4
Figure 3.1:	The Research Process Workflow.	19
Figure 3.2:	A Cast Iron Mould was used to Fabricate the Best-Performing Fire-Retardant Board core.	24
Figure 3.3:	The Size and Measurement of the Best-Performing Fire-Retardant Board (All Units in mm).	24
Figure 3.4:	Illustration of a Best-Performing Fire-Retardant Board.	25
Figure 3.5:	A Commercial MgO Board will be used to Compare the Effectiveness of the Prototypes.	25
Figure 3.6:	The Size and Measurement of the Fire Protection Duct (All Units in mm).	26
Figure 3.7:	Illustration of Fire Protection Duct.	26
Figure 3.8:	Schematic Diagram of the Bunsen Burner Test.	27
Figure 3.9:	Graphical Illustration of Experiment Setup for Adhesion Strength Test.	28
Figure 3.10:	Experiment Setup for the Adhesion Strength Test.	29
Figure 3.11:	Schematic Diagram of a Small-Scale Fire Test.	31
Figure 3.12:	Two different diameters (60 mm and 30 mm) of the samples were cast.	32
Figure 3.13:	BSWA Impedance Tube Measurement Systems.	32
Figure 3.14:	The setup of the test.	33
Figure 3.15:	Illustration of the test.	33
Figure 3.16:	Schematic Diagram of a 1-hour Small-Scale Fire Test.	35

Figure 4.1:	The Temperature Increment of All the Samples.	37
Figure 4.2:	Weight Change Percentage of All Samples.	39
Figure 4.3:	The Adhesion Strength of All Samples.	40
Figure 4.4:	Surface Morphology of All Samples Char Layer.	42
Figure 4.5:	Oxygen/Carbon Ratio of All Samples.	44
Figure 4.6:	TGA Curve of each Prototype.	45
Figure 4.7:	Functional Groups of All Samples.	47
Figure 4.8:	Temperature Profiles of Prototypes and the commercial MgO board.	49
Figure 4.9:	P4 showed a Thicked Char Layer than P3.	50
Figure 4.10:	Weight Loss Percentage of the Prototypes and the Commercial MgO board.	51
Figure 4.11:	The stress-strain curve and the prototypes after conducting the test.	53
Figure 4.12:	Temperature Profiles of Prototype P4 and the Commercial MgO board.	56
Figure 4.13:	Weight Loss Percentage of Prototype P4 and the Commercial MgO board.	57
Figure 4.14:	Both sides (T1 and T2) of the fire protection duct were exposed to fire for 1 hour.	58
Figure 4.15:	Temperature Profile of right (T1) and left (T2) sides of the fire protection duct.	59

LIST OF SYMBOLS / ABBREVIATIONS

ρ	Density, kg/m ³
M	Prototype's mass, kg
V	Prototype's volume, m ³
f_b	Adhesion strength, MPa
A	Surface area of the rod, mm ²
E_f	Flexural modulus of elasticity, MPa
L	Interval length between the supporting pins, mm
F	Load applied at a specific point, N
m	Slope of the load-deflection curve, N/mm
ε_f	Strain applied on the sample, mm/mm
σ_f	Stress at the center of the sample, MPa
W_e	The excess sample's weight after the water soaked, g
W_o	The ordinary sample's weight before the water soaked, g
d	Sample's thickness, mm
V	Voltage
E_{SW}	Water absorption of the sample, %
<i>wt. %</i>	Weight percent
b	Sample's width, mm
Al_2O_3	Aluminium Oxide
APP	Ammonium Polyphosphate
$CaCO_3$	Calcium Carbonate
CaO	Calcium Oxide
$CaSiO_3$	Calcium Silicate
CES	Chicken Eggshell
CO_2	Carbon Dioxide
EDX	Energy-disperse X-ray Spectroscopy Test
EG	Expandable Graphite
FTIR	Fourier Transform Infrared Spectroscopy Test
H_2O	Water
O/C	Oxygen/Carbon ratio
$Mg(OH)_2$	Magnesium Hydroxide

MgO	Magnesium Oxide
MEL	Melamine
PER	Pentaerythritol
SEM	Scanning Electron Microscopy Analysis
TGA	Thermogravimetric Analysis Test
TiO ₂	Titanium Dioxide
UV	Ultraviolet Ray
VAC	Vinyl Acetate Copolymer Emulsion
W-IB	Water-based Intumescent Binder

LIST OF APPENDICES

Appendix A-1:	EDX result for S1.	78
Appendix A-2:	EDX result for S2.	79
Appendix A-3:	EDX result for S3.	80
Appendix A-4:	EDX result for S4.	81
Appendix A-5:	Sample Calculation of Flexural Stress and Flexural Modulus	82
Appendix B-1:	The difference between prototypes before and after the Bunsen burner test.	83
Appendix B-2:	The sample weight before and after the Static immersion test.	84
Appendix B-3:	The difference between sample before and after the Static immersion test.	84
Appendix B-4:	The difference between prototypes before and after the Half-hour Small-scale Fire test.	85
Appendix B-5:	The difference of prototype P4 before and after the 1- hour Small-scale Fire test.	86
Appendix B-6:	Char layer formed at both sides of the Fire Protection duct to protect the Electrical cable.	86
Appendix C-1:	Silver Award is Obtained in Final Year Project Poster Competition with Certificate and Cash prize of RM 120.	87
Appendix C-2:	Draft of a Conference Paper to be Submitted in the Local Conference.	87

CHAPTER 1

INTRODUCTION

1.1 General Introduction

Human lifestyles have started to change due to the convenience made by modern technologies. As an example, employees have changed their working environment from outdoor to indoor offices. Instead of working under the natural sunlight, people nowadays spend most of their time in the indoor environment.

In response to human behaviour changes, it is important to understand the purpose of fire protection systems in indoor buildings. When talking about the structure of a building, fire safety always comes to mind. It is essential for businesspeople as fire has an instantaneous response to spread in seconds. Business capital investment in fire protection systems brings a noteworthy benefit as they can reduce damage to the building structure, valuable equipment, important documents, etc.

The basic functions of fire protection systems are to reduce the fire spread rate and increase the human escape time. The common fire-protective appliances are the smoke detector and sprinkler. When the smoke detector detects the fire smoke, the sprinkler will be activated to release the water. Clean agents will replace the water during crucial moments.

A fire protection system can be classified into active and passive. An active fire protection system is a system whereby an action (automatic or manual) will be performed to extinguish a fire. It can be automatic, such as the sprinkler releasing the water when the temperature rises, whereas a fire extinguisher is an example of a manual method to reserve the escaping time and reduce the property's damage. Besides, passive fire protection systems are equally essential in fire safety as they are the structure of the building that resists fire spread. Examples include fire-resistant doors, smoke dampers, firewalls, etc. One of the influential factors that determine fire protection performance is the construction materials. For example, a fire-rated door has a good layer of thermal protection because it has flame-retardant additives, fillers, and a binder.

A fire-retardant board is one of the passive fire protection systems. It can resist the spread of fire and withstand fire radiation due to its high thermal insulation and great absorption of heat (Sunrock, 2022). These characteristics can maintain a low temperature on the back of the board, thus increasing the human escaping time to a safer place. Due to the integrity itself, the fire-retardant board can serve as a fire protection barrier in the building compartments (Figure 1.1), an electrical cable encasement (Figure 1.2), and smoke and ventilation extraction ductwork (Figure 1.3).



Figure 1.1: Fire Protective Compartment (Panel Built Incorporated, 2022).

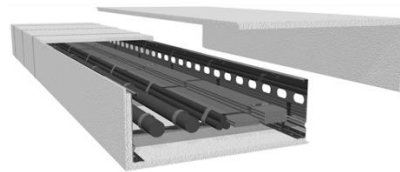


Figure 1.2: Electrical Cable Encasement (Benarx, 2022).



Figure 1.3: Extraction Ductwork (Fire Trace, 2022).

To determine the fire resistivity, the system must fulfil three criteria stated in the European test standards, which are R (Load-bearing function), E (Integrity), and I (Insulation). R defines the capability of a structure to handle the weight without breaking it down. E describes the potential to stop the

penetration of hot gases and flames, whereas I gives the meaning of regulating the rising temperature on the cold side of the system. Next, the ability of the fire resistance is indicated in minutes. For instance, a fire-retardant board that can withstand a fire for up to 120 minutes can be classified as "R 120," and a fire-resistant door that remains the cold temperature on the back of the door for 90 minutes is expressed as "EI 90" (Promat, 2019).

Nonetheless, the performance of the fire-retardant board during a fire test is based on the complicated flow of temperatures and some mechanical properties that occur on the board. So, the fire resistance classification is based on the thickness of the boards, the type of boards, and the composite materials.

There are severe flame-retardant fillers (i.e., aluminium oxide, calcium silicate, chicken eggshell) that affect the resistivity of the fire-retardant board. Aluminium Oxide, Al_2O_3 , is widely used in industry because of its inorganic flame-retardant properties, which enable it to emit non-toxic gases. Apart from that, Al_2O_3 will lower down the temperature of the burning area, decreasing the effectiveness of flammable gases, and reducing smoke.

Calcium silicate, CaSiO_3 , is widely used as impressive insulation in thermal and acoustic systems and provides outstanding resistance to impact and moisture (Promat, 2022). Thus, it is commonly used in building structural components.

Chicken eggshell serves as a natural material as it comprises zinc, potassium, and nitrous that can greatly reduce the smoke emission and heat release by expanding the intumescent char (Xu, et al., 2018).

1.2 Importance of the Study

A fire protection duct can be developed by the combination of fire-retardant boards. The ductwork is significant in providing a safe condition for the electrical circuits. During a fire outbreak, the fire protection duct as shown in Figure 1.4 will resist the penetration of the fire or high temperature to the wiring cables as the cable is necessary to transmit the electricity for fire-protective electrical appliances such as the emergency power systems to protect the people and the building (CWS, 2022).



Figure 1.4: Fire Protection Duct (OBO Bettermann, 2022).

According to Connell (2009), the electrical wiring stored in the fire ductworks will provide electrical power to the active fire protection systems (i.e., smoke extraction fan) and firefighting (i.e., fire alarm system). For instance, the electrical cables provide power supplies to the fire alarm system. Although the alarm is equipped with two 12 V backup batteries (Koorsen Fire & Security, 2020), the electricity supplies ensure it operates normally throughout the day. When the smoke detector detects a fire or smoke, the alarm will sound and alert the occupants about the fire hazard.

Therefore, a fire protection duct ensures the fire protection system can function properly to provide fire protection and extend evacuation times. Other than that, the results from this study may have an impact on the industry by selecting the right amount of suitable materials to improve the characteristics of the commercial fire-retardant board and fire protection duct.

1.3 Problem Statement

Fire-rated MgO board is a popular fire protection board as it consists mainly of a magnesium oxide core for fire-resistance protection when compared with common construction materials such as plywood and fibreboard.

Other than fireproofing, MgO boards perform well in sound insulation. This is important in a building not just to provide a good atmosphere but also to reduce the clamorous sound. For example, the transmission of electricity may create a loud sound and cause a disturbance. The use of a MgO board could separate the sound from the compartment to provide a silent environment.

However, a MgO board possesses some drawbacks, like the composition's low resistance to water vapor and poor restraint from the moisture

surrounding it (Tailor, 2020). MgO board was manufactured by some chemical compositions, which include chloride salts. When the MgO board is exposed to the moisture environment for a long period of time, the moisture that collects on the pore of the board will saturate the chemical ions, thus causing the MgO board to lose its structure (Rode et al., 2017). Additionally, it has a low resistance to fire. The commercial MgO board was unable to endure a high temperature for at least 10 minutes during the half-hour small-scale fire test because of its poor integrity when exposed to a high-temperature flame. As a result, the high temperature would cause a damage to the underlying substrate, and the user would have to purchase a new one to replace the damaged MgO board, which is not economically feasible for the user.

The excessive use of MgO boards has created a notable environmental problem. Research says that the estimated number of MgO boards produced a year is more than 30 billion square feet (Kubba, 2017). Although it can be recycled and reproduced into a brand-new product, this is not practical for the company as extra workflow will be implemented.

In order to further enhance the protection of the underlying substrate and overcome the shortage of poor fire and water resistivity, this project aims to develop the W-IB to replace the currently available and widely used MgO board.

1.4 Aim and Objectives

The reason for conducting this analysis is to analyse the capability of fire-retardant boards and improve their quality and reliability. The results of the study can be used as a reference to improve the capabilities of the fire-protection duct. The objectives to reinforce the aim are given as:

- (i) To formulate the water-based intumescent binder (W-IB) and develop the fire-retardant board for the fire protection duct.
- (ii) To analyze the characteristics of the sample using Scanning Electron Microscopy (SEM) analysis, Energy-disperse X-ray (EDX) Spectroscopy test, Thermogravimetric Analysis (TGA) test, and Fourier Transform Infrared (FTIR) Spectroscopy test.

- (iii) To identify the performance of fire protection duct in terms of fire resistance test, water resistance test, sound insulation test, and mechanical properties test.

1.5 Scope and Limitation of the Study

Different compositions were used to construct a fire-retardant board. For example, flame-retardant additives (i.e., ammonium polyphosphate, APP; pentaerythritol, PER; melamine, MEL; expandable graphite, EG), fillers (such as chicken eggshell CES, titanium dioxide TiO_2 , calcium carbonate CaCO_3 , magnesium hydroxide $\text{Mg}(\text{OH})_2$, calcium silicate CaSiO_3 , aluminium oxide Al_2O_3), and binder (such as vinyl acetate copolymer emulsion VAC and acrylic emulsion copolymer) will characterise the fire resistivity, chemical, physical, thermal, and mechanical aspects. Next, a series of testing methods such as the Bunsen burner test, static immersion test, adhesion strength test, SEM analysis, EDX test, TGA test, and FTIR test were conducted to characterise the W-IB. After that, testing for fire-retardant board prototypes, such as a half-hour small-scale fire test, a density measurement test, a sound insulation test, and a three-point flexural test, were carried out to choose the best-performing composition before making the best-performing fire-retardant board. Furthermore, a 1-hour small-scale fire test and the density measurement test were performed to differentiate the effectiveness of the best-performing fire-retardant board with the commercial MgO board. Lastly, the small-scale fire protection duct was assembled using the best-performing fire-retardant board before carrying out the 1-hour small-scale fire test to evaluate the duct's ability to protect the electrical cable store underneath. Some limitations exist in this research, which include:

- (i) A variety of flame-retardant materials with different compositions are used in the market to construct fire-retardant boards. Therefore, the results of the research may differ from the market's products.
- (ii) The brand/manufacturer of the testing equipment used in this research may differ from other research work, thus the results might be slightly different from those of another researcher.
- (iii) As a consequence of the limitations of lab apparatus and the environment, a small-scale fire test will be conducted to replace

a full-scale fire test. In this manner, the outcomes obtained from the small-scale fire test might differ from those obtained from a full-scale fire test.

1.6 Contribution of the Study

The W-IB used in this research was mixed with halogen-free flame-retardant materials. These materials released a lesser amount of smoke and toxic gas as compared with the halogen-based materials. Besides, the halogen-free flame-retardant materials (e.g., APP, PER, MEL) would undergo an environmentally friendly process such as carbonization to release a small amount of carbon dioxide, CO₂ to prevent the W-IB from being propagated by the hot gas and create a char layer that serves as a barrier that restricts the transmission of heat and mass. These processes in turn reduce the damage to the material underneath (e.g., steel plate).

Other than that, the cost required to cast the fire-retardant board using the W-IB formulations is lower than the commercial fire resistance board. The main materials found inside the formulations (e.g., Al₂O₃, CES, TiO₂) allow a low-cost ability to make a fire protection duct. The detailed cost analysis is presented in Section 4.6 of this research report.

In short, using non-halogenated-based flame-retardant materials offers environmentally friendly properties as well as reducing the cost required to fabricate a fire protection duct.

1.7 Outline of the Report

There are five chapters in total, and each chapter has a number of sub-chapters, which are listed as follow:

Chapter 1—Introduction: This section includes the background and the importance of the study, the aim and objectives of the experimental research, the problem statement, the limitations of the research, and the contribution of the research.

Chapter 2—Literature Review: This section discussed the research works done by numerous researchers in the fire-retardant industries. The evaluations of each ingredient utilized in the analysis, such as flame-retardant additives, fillers, material, and water-based polymer binders, were also explained in this research.

Chapter 3—Methodology: This section explains the techniques used to evaluate the fire resistivity, chemical, physical, thermal and mechanical aspects, as well as the sound absorption rate and the three-point flexural strength of the W-IB and the fire-retardant board prototypes.

Chapter 4—Results and Discussion: This section consists of the illustration, investigation, and comment of the information and outcomes collected from each testing method. Other than that, a cost analysis of constructing a fire-retardant board using the preferred compositions would also be discussed.

Chapter 5—Conclusion and Recommendations: The chapter summarized the main findings for each testing method. The recommendations from the study would also be discussed in this section.

CHAPTER 2

LITERATURE REVIEW

2.1 Introduction

This section will focus on the important parameters of the fire resistivity, chemical, physical, thermal, and mechanical strength of the board with the inclusion of flame-retardant additives, fillers, polymer binder, and materials.

Referring to Jong, et al. (2019), the composites used to create a fire-retardant board and fire protection duct are flame-retardant additives that bond with some fillers, polymer binder, and vermiculite. All of the parts will make the fire-retardant board more resistant to high temperatures and improve its sound insulation, water resistance, and mechanical strength.

2.2 Flame-retardant Fillers

Flame-retardant fillers are important in terms of fire protection. They can reduce the fire growth parameters (e.g., fire, fuel, and oxygen) in the combustion area without using a halogenated compound. In addition, the development of flame-retardant fillers is used to replace the halogenated solvents that will produce toxic gases during decomposition. Thus, an appropriate amount of flame-retardant fillers will safeguard against fire damage and enhance fire resistivity (Jong, et al., 2019).

2.2.1 Chicken Eggshell Powder

Chicken eggshell, CES, is a biodegradable by-product that will become a waste product that pollutes the environment. This kind of waste will generate a series of environmental problems, such as releasing a pungent smell that disrupts the citizens nearby.

The United States of America (USA), China, and India serve as major nations that enroll in the mass production of chicken eggs. Due to less knowledge of chicken eggshell's benefits, these countries face a serious issue in handling food waste. To deal with the ecological concern, society started to consider the potential of the CES as it consists of some organic and inorganic compounds that can be applied to a commercial product and reduce the

manufacturing price of the product due to its high availability as well as increase the usage of the chicken eggshell.

According to Beh, et al. (2019), the eggshell consists of 95 % calcium carbonate and 5 % sulphated polysaccharides and other proteins. A large amount of availability and attractive chemical compositions are capable of providing shielding in terms of fire resistance and mechanical strength.

Besides, the CES offers attractive characteristics such as being lightweight, eco-friendly, and available in bulk quantity. It has a low density of 0.4236 g/cm^3 as claimed by Toro, et al. (2007). Other than that, the CES also provides a higher crystallinity of 48 % as compared with the commercial CaCO_3 of 46 %.

2.2.2 Magnesium Hydroxide

Magnesium hydroxide, Mg(OH)_2 , has recently been applied as a flame-retardant filler to replace halogen-based fillers. According to Xu, et al. (2011), Mg(OH)_2 absorbs a large amount of heat, produces a large amount of char, neutralises toxic burning gases, and reduces the amount of smoke.

Because of its high melting point of $300 \text{ }^\circ\text{C}$ and decomposition to produce magnesium oxide, MgO , and water, H_2O , Mg(OH)_2 is commonly used with halogen-free materials (e.g., plastic and rubber). The H_2O will cover the materials from direct penetration by fire, lower the air level, and dilute the combustible gases. Additionally, MgO will generate a fire protective barrier on the halogen-free materials as claimed by Li, et al. (2014).

Mg(OH)_2 exists in the form of a white powder with 58.32 g/mol of molecular weight and 2.36 g/cm^3 of density (Sigma-Aldrich, 2022). Following that, Mg(OH)_2 has a low solubility in sodium hydroxide but is highly soluble in a strong acid solution, as many researchers have noted.

According to (Zhang, et al., 2018), the decomposition of Mg(OH)_2 can absorb up to 44.8 kJ/mol of heat and performs well in slowing down the polymer's increment temperature during decomposition. Besides, the MgO covers the polymer and prevents the burning material from receiving oxygen, which consequently lowers the ability of heat transfer to the material. Lastly, the H_2O is released to reduce the combustible gases in the burning area. Aside from that, the decomposition of Mg(OH)_2 does not produce harmful gases and

instead neutralises acidic substances. Therefore, it is an acceptable fire-retardant filler that contributes to the environment.

2.2.3 Titanium Dioxide

Titanium dioxide, TiO_2 , is an alkaline metal that exists in the form of a solid white powder and is insoluble in water but possesses high solubility in concentrated acids. It is odorless, non-toxic, and incombustible, providing a high density of 4.26 g/cm^3 . Apart from this, it consists of 79.9 g/mol of molecular weight with a high melting point and boiling point of $1850 \text{ }^\circ\text{C}$ and $3000 \text{ }^\circ\text{C}$, respectively (Merck, 2022).

Wang, et al. (2017 cited in Oliveira, et al., 2021) reviewed how combining TiO_2 with other fillers can slow the spread of fire. This is because TiO_2 serves as a heat sink to disturb the combustion cycle (Schindler and Hauser, 2014 cited in Poon and Kan, 2015). Besides, TiO_2 helps to generate a stronger, larger, and expanded char layer to strengthen the fire-resistivity of the product (Chaisaenrith, et al., 2021). Unlike other fillers, the existence of TiO_2 will not compensate for the tensile strength of the product, but instead absorb the UV light for better surface texture (Lam, et al., 2012 cited in Poon and Kan, 2015).

On the other hand, Gutenmann and Lisk (1975 cited in Poon and Kan, 2015) proposed that adding flame-retardant chemicals may have a serious effect on the marine system. Schindler and Hauser (2014 cited in Poon and Kan, 2015) further explained that the existence of phosphorous compounds in the wastewater will disrupt the ecosystem. By adding TiO_2 , the side effect mentioned above can be lessened, and the amount of formaldehyde released can also be cut.

Furthermore, Montazer and Harifi (2018 cited in Oliveira, et al., 2021) claimed that metal oxides (i.e., TiO_2) can protect highly flammable products by helping to stabilise the material's components during high temperatures (Li, et al., 2015 cited in Jong, et al., 2019). Other than that, the use of pigment-grade TiO_2 allows the surface of the product to provide good opacity by scattering the visible light. As a result, TiO_2 can be used as a colourant to create an attractive surface.

2.2.4 Calcium Carbonate

Calcium carbonate, CaCO_3 can effectively lower the surrounding temperature by emitting the CO_2 and reduce the surrounding temperature during the endothermic decomposition (Merk, et al., 2016 cited in Pondelak, et al., 2021). Besides, CaCO_3 is an eco-friendly flame-retardant as it would not cause environmental hazards or significant causes of death or injury to humans.

Hermansson, et al. (2003 cited in Karlsson, et al., 2009) claimed that the properties of the flame retardant are significant during the condensation phase. When degradation occurs, the release of intumescent gases and calcium ions forms cross-linking ions, which can increase the viscosity of melting and decrease the gas moving rate. The overall effect will be increased when the carbonate reacts with the binder, such as ethylene vinyl acetate (EVA).

CaCO_3 has 100.09 g/mol of molecular weight, 2.93 g/cm³ of density, and can withstand a high temperature of up to 800 °C before degradation. It exists as a white and odourless powder or crystals (Sigma-Aldrich, 2020).

2.2.5 Calcium Silicate

Calcium silicate, CaSiO_3 , exists as an off-white powder at room temperature that consists of 116.16 g/mol of molecular weight and 2.92 g/cm³ of density. It performs well in heat insulation as it starts to melt around 1540 °C (Sigma-Aldrich, 2021).

CaSiO_3 will protect the structures of the building, such as steel, timber, concrete, etc., and serve as an independent component, such as ductwork, flame-retardant partition walls, and ceilings. CaSiO_3 is famous in the industry owing to its great thermal insulation, high mechanical intensity, moisture resistance, and free from corrosion (Promat, 2022). So, it is well-known on the market as a calcium silicate board that provides fire protection, sound insulation, and mechanical strength.

Research done by Chen, et al. (2012) stated that the combination of calcium silicate board and gypsum board can effectively withstand a high temperature during the full-scale fire test up to 92 minutes before the structure fails. A thick calcium silicate board with a high amount of CaSiO_3 is most likely to extend fire protection as more spaces are available for the spread of heat on the board.

2.2.6 Aluminium Oxide

Aluminium oxide, Al_2O_3 , performs well in mechanical, thermal, and chemical properties. For chemical quality, it consists of 101.96 g/mol of molecular weight, 4.00 g/cm^3 of density, and is incorporated with a high melting point and boiling point of $2040 \text{ }^\circ\text{C}$ and $2980 \text{ }^\circ\text{C}$, respectively (Sigma-Aldrich, 2021).

Besides, Al_2O_3 will undergo a series of activities such as exothermic, decomposition, and self-sustaining when a specific temperature with the proper pressure is achieved. Thus, the thermal energy can initiate the reaction of the Al_2O_3 .

Next, Al_2O_3 is free from corrosion. A protective layer will be formed when oxygen is bonded with aluminium to prevent oxidation. This characteristic increases the mechanical strength of Al_2O_3 . As a consequence, Al_2O_3 is generally used as the main component in force and military equipment such as body armour breastplates, bulletproof vehicle bodies, windows, etc.

2.3 Flame-retardant Materials - Vermiculite

The size of the vermiculite will expand when the surrounding temperature is high enough to reduce the heat flow of the object. Thus, it is well known in the construction field.

The vermiculite is formed naturally from the weather and groundwater (The Vermiculite Association, 2022). It has 223.28 g/mol of molecular weight and 2.4 g/cm^3 of density. It is stable (chemical inertness) and has a high melting point of $1350 \text{ }^\circ\text{C}$ (Chemical Book, 2017). Aside from that, vermiculite emits non-toxic gasses, has a high expansion rate, and contains cation exchange, which is commonly used in the field of high temperature.

The size will expand 8–30 times during the conversion of water to steam and form a layer of air between the lamellae by absorbing the surrounding moisture, which makes the vermiculite become a highly porous material (expanded vermiculite) with a loose structure and soft texture (Zhou, et al., 2013 cited in Li, et al., 2021). Thus, vermiculite is widely used in construction with low density (lightweight), high insulation of heat (heat conductivity of $0.04\text{--}0.12 \text{ W/m}\cdot\text{K}$), and good sound insulation and absorption (Rashad, 2016 cited in Rabello & Ribeiro, 2021).

2.4 Binder

2.4.1 Vinyl Acetate Copolymer (VAC)

Vinyl acetate copolymer (VAC) emulsion is widely applied in the manufacturing and construction areas due to its high-quality emulsions, which provide good flexibility, resistance to moisture conditions, and good adhesion strength. Besides, VAC creates a strong, flexible, and adhesive film. For example, VAC has a strong adhesion force with aluminium, which is widely used as a coating (Mallard Creek Polymers, 2021).

Yew, et al. (2018) say that VAC can serve as a flame-retardant binder that has a satisfactory expansion rate, promotes the char layer as a protective barricade, and restricts the fire spreading to the substrate. On the other hand, VAC (water-based) possesses less flammability and is more ecological in terms of releasing fewer toxic gases into the environment when compared with solvent-based (Wang and Yang, 2012).

Although VAC holds the properties of the char formation, it should not be used alone as it shows high flammability. Thus, flame-retardants (i.e., Al_2O_3 , $\text{Mg}(\text{OH})_2$) can be added to promote the fire retardancy of the VAC (Xu, et al., 2022).

2.4.2 Acrylic Emulsion Copolymer

Acrylic emulsion copolymer is always used in the flame-retardant industry due to its well-performed water-based fireproof characteristic. Research done by Park, et al. (2021) showed that the acrylic emulsion copolymer has a great bond with the flame-retardant additives and fillers. It has good compatibility with additives and fillers that can release a soft and dense char layer after burning. Besides, it shows good fire and heat insulation, as well as yielding positive results in water resistance and storage ability. Thus, it has always been applied on the surface of the base metal to improve the overall flame retardancy (Mei Wang Chemical, 2022).

2.5 Flame Retardant Additives

The non-halogen flame-retardant additives have become popular in the fire and chemical industry due to the properties of the retardation of fire and hot flame

to reduce the penetration of hot air to the solids inside. This process can be done by the development of a char layer from the additives (Horrocks, et al., 2001 cited in Sun, et al., 2020). Flame-retardant additives consist of an acid source of APP, a carbonization agent of PER, and a blowing agent of MEL which will generate a char layer on the sample during the decomposition of the additives (Sun, et al., 2020). Chemically, the carbon can lessen the heat of combustion of the samples, and reduce the emission of toxic smoke (Mogan, et al., 2013 cited in Sun, et al., 2020). Physically, the char layer is formed to act as a barrier to control the thermal flow of the material and slow down the degradation (Troitzsch, 1990 cited in Thirumal, et al., 2010).

2.5.1 Ammonium Polyphosphate (APP)

The characteristics such as water solubility and the melting point of APP depend on the degree of polymerization. For example, a low polymerization degree ($n \leq 100$, crystalline form I) possesses high solubility in water with a low melting point of 150 °C, whereas a high polymerization degree ($n \geq 1\ 000$, crystalline form II) performs poorly in water soluble with approximately 0.1 g/mL and with a high melting point which only starts to degrade above 300 °C.

When APP is combined with materials consisting of oxygen and/or nitrogen, the formation of char will occur. At elevated temperatures, the degradation of APP releases hydroxyl groups and produces polyphosphoric acid with ultraphosphate. These acids and alkalis will increase the dehydration process of the materials to form char residues. (Fu, Song and Liu, 2017).

APP performs well in char forming and generating a cross-linking skeleton on the char layer during the decomposition of phosphate compounds (Zhang, et al., 2020 cited in Yin, et al., 2021). Other than that, APP is lighter, cheaper, and easier to process when compared with others (Lim, et al., 2016 cited in Liu, et al., 2021). APP commonly exists in white crystal or powder form. It has a molecular weight of 97.01 g/mol, 1.9 g/cm³ of density, and a decomposition temperature of more than 275 °C (Clariant, 2016).

The amount of APP added should be take into consideration. Guo, et al. (2020 cited in Cui, et al., 2021) carried out research saying that excessive APP will lead to a deduction of mechanical properties such as difficulty in constructability and poor compatibility.

2.5.2 Pentaerythritol (PER)

Pentaerythritol (PER) is always used with APP in flame-retardant applications. Although MEL serves as a blowing agent, APP can be used as both the acid source and blowing agent (Wang, et al., 2015), while PER is a carbonization/char forming agent that plays a key role in char forming. When combustion happens, the system experiences esterification and carbonization (Hendrickson and Connole, 1995; Enescu, et al., 2013 cited in Wang, et al., 2017) to generate a char layer that can resist the heat and mass transfer as mentioned earlier.

PER has 136.15 g/mol of molecular weight and 1.395 g/cm³ of density. It exists as a white solid powder that melts at a temperature of 260.5 °C and boils at 276 °C (National Center for Biotechnology Information, 2022).

2.5.3 Melamine (MEL)

Melamine (MEL) consists of a high amount of nitrogen (Xu, et al., 2019). When the temperature reaches above 200 °C, MEL will vaporise to reduce the concentration of the surrounding fuel gases and oxygen. Furthermore, it decomposes at 345 °C to form a thermally stable condensate (Price, et al., 2002, cited in Riyazuddin, et al., 2020). During combustion, MEL releases inert gases such as ammonium and nitrogen to impact the combustion cycle by reducing the level of combustible gases. Other than that, MEL can absorb a high amount of heat, up to 470 kcal/mol, during its decomposition, which allows it to become a heat sink during combustion. In addition, the small particle size allows the MEL to serve as a UV absorber (Flame Retardants, 2022). Lastly, MEL has a number of benefits, such as a low price, good fire resistance, and the ability to stop fumes.

2.5.4 Expandable Graphite (EG)

Expandable graphite (EG) is one of the most essential fillers in the flame-retardant area. It has been widely used in polymers to reduce or eliminate the release of toxic gases. Due to its high heat and electrical conductivity, it provides some service in the automotive, electrical, electronic, and fire safety industries.

EG is becoming familiar in the fire safety industry due to its attractive characteristics, such as its high flammability and competitive price offer in the market. EG can be obtained from the graphite interlayer (Cheng, et al., 2022), and it has been manufactured with sulfuric acid, H_2SO_4 , and nitric acid, HNO_3 , which are inserted into the crystal structure of the graphite to allow the EG to expand perpendicularly to the carbon layers in the crystal structure when exposed to a heat source (Wang, Han and Ke, 2006).

Tomiak, et al. (2021) say that EG can release a high expansion rate and a thermally stable char layer. This residue will effectively slow down or pause the fire spreading from the flame to the substrate, reduce the penetration of oxygen, and lessen the mass transfer of the molecular weight to the gas phase.

EG, with 12.011 g/mol of molecular weight and 2.26 g/cm³ of density, has a melting point of 3652–3697 °C (Sigma-Aldrich, 2023). It exists as a dark grey powder at room temperature.

2.6 Summary

Many researchers have experimented by highlighting the properties of the flame-retardant additives, fillers, materials, and binder on the impact of fire-retardant products. Based on the researcher's reviews, the properties of the fire-retardant board will be affected by the amount (weight percentage), particle size, as well as the compositions of the additives, fillers, materials, and binder added. Besides, some of the flame-retardant additives cannot be used alone but have to be combined with other additives or fillers to provide fire protection. Therefore, using the right amount of composites with suitable particle sizes is important in this experiment to improve the performance of the fire-retardant board. Other than that, a series of sample characterizations such as the SEM test, the EDX test, the TGA test, and the FTIR test were used to analyse the structure and performance of the samples. In short, this experimental research has a lot of potential to find a better way to put together the fire-retardant board and the fire protection duct so that they work better.

CHAPTER 3

METHODOLOGY AND WORK PLAN

3.1 Introduction

In this section, samples and prototypes were prepared to perform a series of testing methods to analyse their performance in respect of fire resistance, water repellence, mechanical strength, physical properties, and thermal properties. Testing methods such as the Bunsen burner test, static immersion test, and adhesion strength test were executed to examine the characteristics of the W-IB in respect of fire protection, water repellence, and mechanical strength. Next, sample characterization tests such as the SEM test, the EDX test, the TGA test, and the FTIR test were conducted to determine the physical and thermal characteristics of the W-IB. Furthermore, small-scale fire test, density measurement test, sound insulation test, and three-point flexural test were conducted to analyse the performance among the prototypes. After that, a 1-hour small-scale fire test were performed to analyse and correlate the properties of the best-performing fire-retardant board with the commercial MgO board before making a fire protection duct. Lastly, the properties of the fire protection duct in resisting the fire penetration and protecting the electrical cables were evaluated through a 1-hour small-scale fire test.

3.2 Process Flowchart

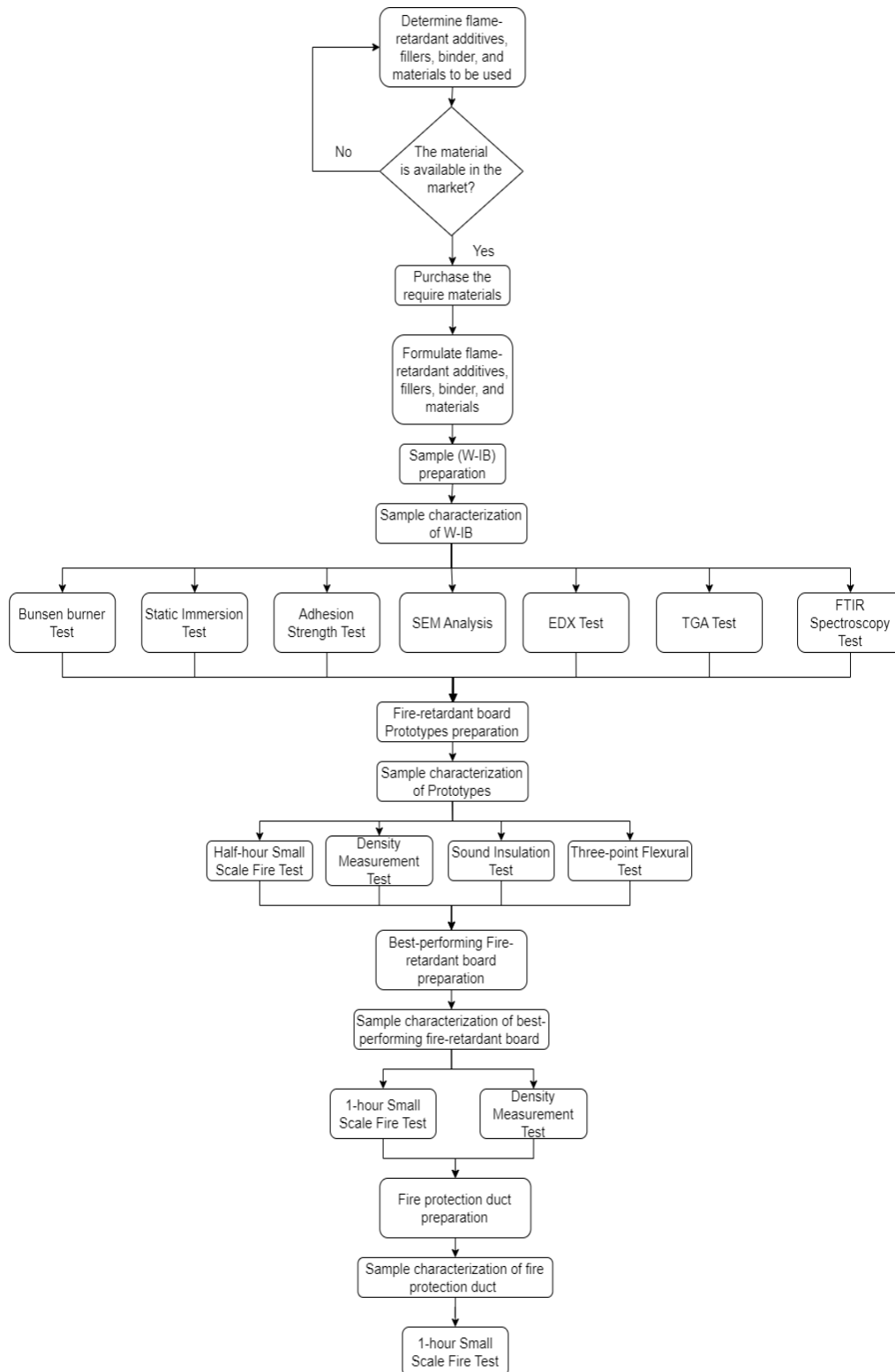


Figure 3.1: The Research Process Workflow.

3.3 Materials Preparation

Four W-IB with different compositions were prepared and formulated as shown in Table 3.1, whereas four prototypes were fabricated afterwards by following the compositions of the samples, with the addition of vermiculite as shown in Table 3.2.

Table 3.1: Samples' compositions.

Composition (wt. %)	Samples			
Flame-retardant Additives	S1	S2	S3	S4
APP	30	30	30	30
PER	10	10	10	10
MEL	10	10	10	10
EG	-	-	-	2
Flame-retardant Fillers				
Al ₂ O ₃	-	3.0	-	2.0
CaCO ₃	-	-	3.5	-
CaSiO ₃	4.0	-	-	-
Mg(OH) ₂	2.0	-	-	-
CES	-	3.0	18.5	3.0
Flame-retardant Filler (Pigment)				
TiO ₂	4.0	4.0	8.0	3.0
Binder				
Vinyl Acetate Copolymer Emulsion (VAC)	40	40	-	40
Acrylate Emulsion Copolymer	-	-	20	-

Table 3.2: Prototypes' compositions.

Compositions (wt. %)	Prototypes			
Flame-retardant Additives	P1	P2	P3	P4
APP	30	30	30	30
PER	10	10	10	10
MEL	10	10	10	10
EG	-	-	-	2
Flame-retardant Fillers				
Al ₂ O ₃	-	3	-	2
CaCO ₃	-	-	3.5	-
CaSiO ₃	4	-	-	-
Mg(OH) ₂	2	-	-	-
CES	-	3	18.5	3
Flame-retardant filler (Pigment)				
TiO ₂	4	4	8	3
Binder				
Vinyl Acetate Copolymer Emulsion (VAC)	40	40	-	40
Acrylate Emulsion Copolymer	-	-	20	-
Flame-retardant materials				
Vermiculite (mL)	400	400	600	150

In this experiment, flame-retardant additives (APP, particle size $\leq 100 \mu\text{m}$) was purchased from Clariant Plastics & Coating USA Inc., whereas PER, MEL, and EG were purchased from Sigma-Aldrich (M) Sdn. Bhd. Next, the fillers such as TiO₂, Mg(OH)₂, and CaCO₃ were purchased from Ever Gainful Enterprise Sdn. Bhd. (R&M Chemicals). Al₂O₃ with a particle size of $106 \mu\text{m}$ and CaSiO₃ (particle size $7.0 - 10.0 \mu\text{m}$) were purchased from Sigma-

Aldrich (M) Sdn. Bhd. Besides, the VAC binder, acrylate copolymer emulsion, and vermiculite (particle size 2-3 mm) were purchased from Sigma-Aldrich (M) Sdn. Bhd. Lastly, the defoamer was acquired from DChemie Malaysia. Among all the compositions, CES (particle size 300 μm) was prepared by removing the shell membrane, thoroughly cleaning the eggshell, and drying it in the oven for 12 hours at 90 °C. After that, it was mechanically granulated into smaller particles, followed by milling the particle to get a micronized particle size. Lastly, an EDAX S3400-N SEM machine was used to measure the CES's particle size.

3.4 Sample and Prototype Preparation

While preparing the flame-retardant samples (W-IB), the amount of composition was followed in Table 3.1. Next, the compositions and some water (approximately 20–25 wt.%) were poured into the high-speed disperse mixer to be mixed and blended for 30 minutes at room temperature. The reason for adding the water was to prevent too much viscosity in the compositions. Then, a small portion (approximately 5 wt.%) of defoamer was added to remove the foams and bubbles in the compositions. The defoamer has a low viscosity and will spread rapidly on the foamy surface. It will then destabilise the foam lamellas, causing the air bubbles to rupture (Kakhia, 2023). Besides, polyethylene terephthalate (PET) polyester fibre was also added to the fire-retardant board prototypes, with compositions of about 1.5 wt. %. PET textile fibre can increase the overall strength of the prototypes, allow low shrinkage, and provide heat stability in the compositions. The characteristics that PET possesses are mainly due to the presence of ethylene glycol and terephthalic acid. The polymer chains that aligned in an orderly arrangement with the long aromatic ring found in the terephthalic acid make the PET stiffer and stronger.

In the testing methods, more than one specimen was prepared for each sample in order to improve the precision and accuracy of the experiment data. The results of the static immersion test and adhesion strength test, for instance, were calculated by averaging the data from two specimens. However, due to the limitations of the flame-retardant materials available, several testing methods that call for a large sample size (e.g., a Bunsen burner test, a half-hour small-scale fire test, a three-point flexural test, a one-hour small-scale fire test) make

it challenging to prepare more than one specimen for each sample. Besides, some of the sample characterizations of W-IB (e.g., SEM/EDX test, TGA test, and FTIR test) provide a qualitative result that shows the surface morphology and oxygen/carbon (O/C) ratio, the residue weight, and the functional groups that exist in the samples, respectively. As a result, the testing methods are unable to give any quantifiable results. Furthermore, the testing methods (e.g., a sound insulation test) revealed that the W-IB produces outcomes that are identical for each formulation. Hence, only one of the W-IB formulations was used in the testing procedure.

In the preparation of fire-retardant board prototypes, the dimensions of the prototypes were 175 mm (length), 175 mm (width), and 12 mm (thickness). The compositions of the core prototypes (P1–P4) were the same as the samples prepared, with the inclusion of vermiculite, as shown in Table 3.2, to improve the fire resistance. The purpose of fabricating four different prototypes was to determine the best-performing composition.

After determining the best-performing flame-retardant composition, a 175 mm × 175 mm × 30 mm fire-retardant board core was cast. A 300 mm × 300 mm × 30 mm cast iron mould was used to cast the core of the best-performing fire-retardant board, as shown in Figure 3.2. Before the moulding process began, the cast iron mould was thoroughly cleaned to prevent any residue from sticking to it. Next, the cast iron mould was disassembled and wrapped with plastic to secure the satisfactory appearance of the board, and also to prevent the composition from sticking to the mould. Once the cast iron mould was prepared, the composition was poured into the mould. Then, the moulding and curing process took place by leaving the mould aside for a week.



Figure 3.2: A Cast Iron Mould was used to Fabricate the Best-Performing Fire-Retardant Board core.

After the moulding and curing processes were completed, the best-performing composition was applied on the surface of the fire-retardant board, as shown in Figure 3.3, whereas Figure 3.4 illustrates of the best-performing fire-retardant board. Lastly, the fire-retardant board was ready to perform a 1-hour small-scale fire test.

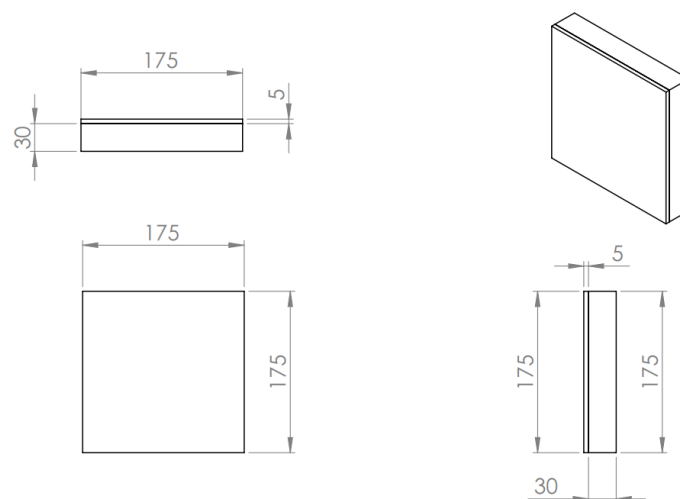


Figure 3.3: The Size and Measurement of the Best-Performing Fire-Retardant Board (All Units in mm).

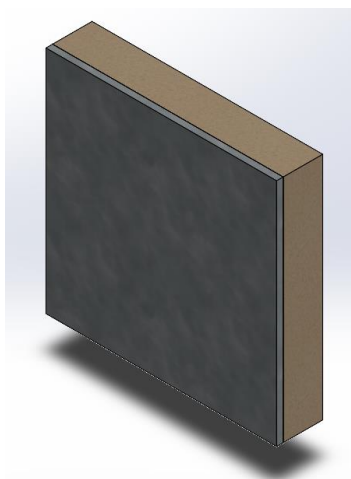


Figure 3.4: Illustration of the Best-Performing Fire-Retardant Board.

A commercial MgO board, as shown in Figure 3.5, was used to make a comparison with the best-performing fire-retardant board in terms of fire resistivity and density. Furthermore, the best-performing fire-retardant board was cut and assembled to make an 85 mm × 50 mm × 60 mm small-scale fire protection duct, as shown in Figure 3.6. The illustration of the fire protection duct is presented in Figure 3.7.



Figure 3.5: A Commercial MgO Board was used to Compare the Effectiveness of the Best-Performing Fire-Retardant Board.

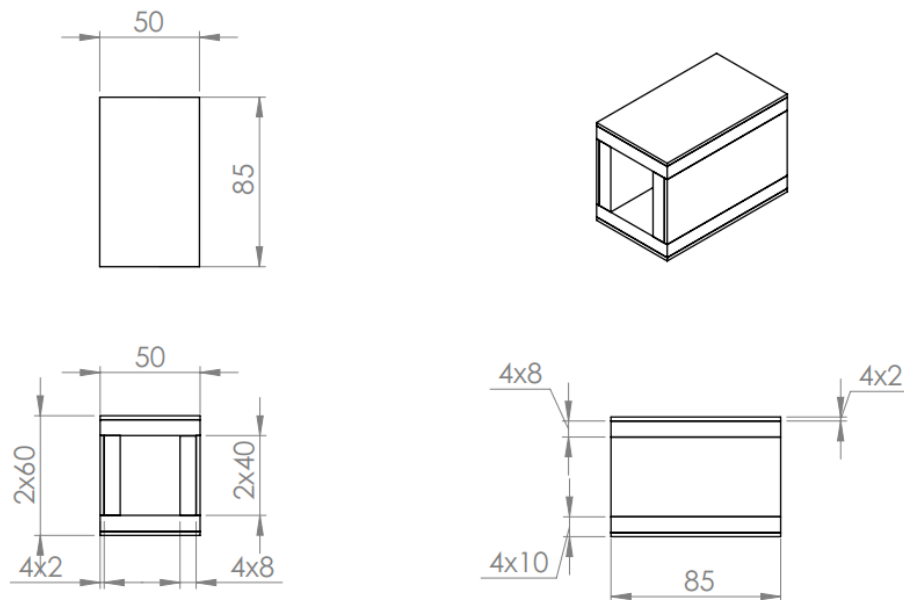


Figure 3.6: The Size and Measurement of the Fire Protection Duct (All Units in mm).

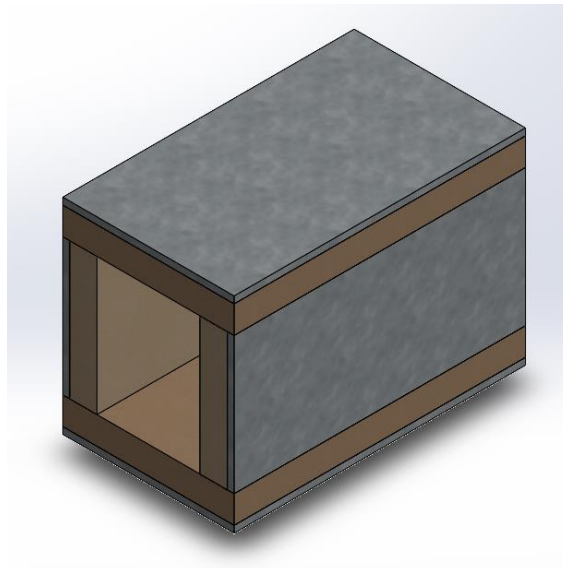


Figure 3.7: Illustration of Fire Protection Duct.

3.5 Testing Methods for Water-based Intumescent binder

3.5.1 Bunsen Burner Test

A 100 mm × 100 mm × 1 mm sample (W-IB) was prepared. Besides, a thermocouple plate was bound to the back of the sample for temperature recording. The k-type thermocouple wire was used to connect the thermocouple plate to the portable digital thermometer. After that, a Bunsen burner flame

spray gun with a gas consumption of 160 g/h was placed in front of the sample at a distance of about 7 cm (interval between the sample and the spray gun). Next, the sample was directed to the flame spray gun with a hot flame of 1000 °C for half an hour to meet the fire-rated design standards. Figure 3.8 illustrates the setup of the Bunsen burner test.

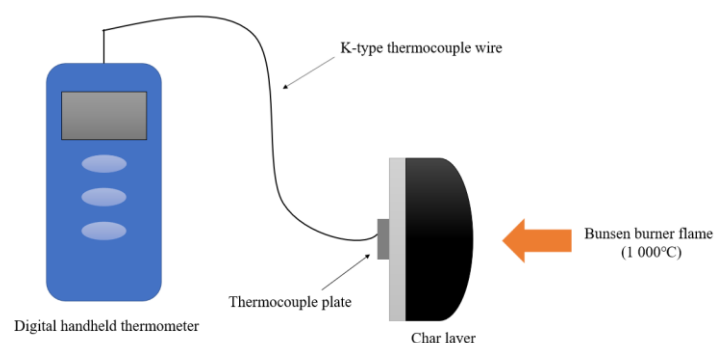


Figure 3.8: Schematic Diagram of the Bunsen Burner Test.

3.5.2 Static Immersion Test

This test determined the sample's water repellence. First, the mixtures were transferred into the plastic mould, which was then allowed to be set away for a week until it was absolutely dry. Next, the mould was taken out and the weight was measured before it was immersed in the water. The water immersion test was carried out for five days. After that, the extra water on the sample was wiped with tissue paper. The sample's weight after being immersed in the water was measured using a weighing machine. Lastly, the formula shown in equation 3.1 was used to figure out the weight change percentage.

$$E_{SW}(\%) = [(W_e - W_o) / W_o] \times 100 \% \quad (3.1)$$

where

E_{SW} = water absorption of the sample, %

W_e = the excess sample's weight after the water soaked, g

W_o = the ordinary sample's weight before the water soaked, g

To calculate the sample's weight change, the sample was measured both before and after it was submerged in water. The smaller the change in the sample's weight, the higher the water resistance.

3.5.3 Adhesion Strength Test

The experiment analysed the adhesive strength of the samples. On one side of the cylindrical rod, a sample coating with a thickness of $2 \text{ mm} \pm 0.1 \text{ mm}$ was applied. Thereafter, the sample coatings were set aside to finish drying. The surface of the dried sample coating was then covered in epoxy glue and adhered to another side of the steel rod. Besides, using the Shimadzu AGS-X in the tensile mode with a 1 mm/min constant rate, two cylindrical steel rods were dragged apart until the coating samples were detached, as shown in Figures 3.9 and 3.10. Last but not least, Equation 3.2 was implemented to define the adhesive strength of the sample.

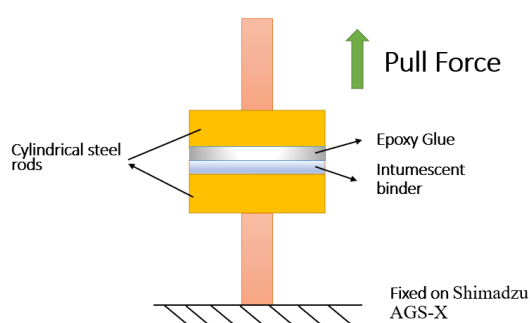


Figure 3.9: Graphical Illustration of Experiment Setup for Adhesion Strength Test.



Figure 3.10: Experiment Setup for the Adhesion Strength Test.

Adhesion strength calculation formula, f_b (MPa):

$$f_b = F / A \quad (3.2)$$

where

f_b = Adesion strength, MPa

F = Peak load applied at rupture, N

A = Surface area of the rod, mm^2

3.5.4 Scanning Electron Microscopy (SEM) Analysis

This test used to analyse and review the samples' surface morphology and interfacial bonding. The analysis test was carried out on a Hitachi S-3400N SEM equipment made by Hitachi High Technologies America, Inc. The char layer collected from the Bunsen burner test were coated with a gold layer to remove the charging effects. The samples were then subjected to a 1 kV low beam energy procedure to reduce the possibility of thermal damage.

3.5.5 Energy-disperse X-ray (EDX) Spectroscopy Test

EDX is frequently conducted with SEM. It is a chemical microanalysis method that used to characterise the elemental composition of the examined microscale

size by using X-rays that are released by the sample. This test's equipment was identical to that used for SEM testing.

3.5.6 Thermogravimetric Analysis (TGA) Test

The TGA test measured the weight of the sample (W-IB) after undergoing a heating process to define the thermal stability of the sample. In this experiment, a PerkinElmer STA 8000 model machine manufactured by PerkinElmer Inc., Waltham, MA, USA, was used to perform a thermal analysis of 5 mg to 8 mg of the samples from 30 °C to 1000 °C by increasing the temperature at 20 °C/min intervals using nitrogen gas. The thermal stability of the sample is classified as good if the residue weight after the heating progress is large.

3.5.7 Fourier-transform Infrared (FTIR) Spectroscopy Test

This analysis evaluated the change in the sample's chemical and molecular structure with the addition of additives, fillers, and binder. The development of the char layers and the specific functional groups were investigated under the wavenumber spectrum from 500 cm^{-1} to 4000 cm^{-1} . The Nicolet iS10 spectrometer was used in this analysis.

3.6 Testing Methods for Prototypes

3.6.1 Half-hour Small-scale Fire Test

The analysis analysed the fire protection among the prototypes P1 to P4 and the commercial MgO board. First of all, a Bunsen burner sprayed a 1000 °C flame on the prototype for half an hour. The temperature increment data was recorded by using a portable digital thermometer. Figure 3.11 represents the setup of the small-scale fire test.

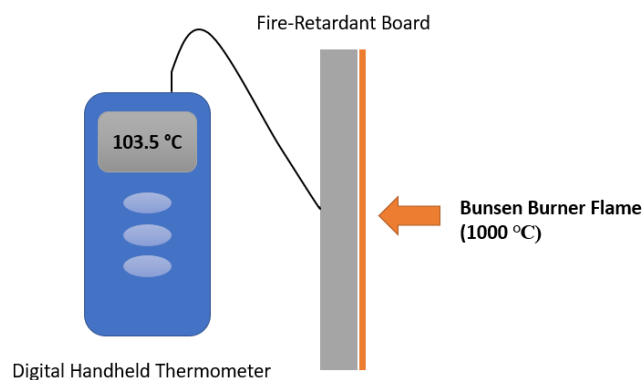


Figure 3.11: Schematic Diagram of a Small-Scale Fire Test.

3.6.2 Density Measurement Test

The test is essential to determining the overall density of the prototypes and the commercial MgO board before and after the small-scale fire test. The density of the testing samples can be calculated by weighing them on a weighing machine and calculating their total volume. The equation to calculate the density is shown in equation 3.3:

Density calculation formula, ρ (kg/m^3):

$$\rho = M / V \quad (3.3)$$

where

ρ = prototype's density, kg/m^3

M = prototype's mass, kg

V = prototype's volume, m^3

3.6.3 Sound Insulation Test

A sound insulation test (Impedance Tube Test) was performed in this experiment to measure the sound absorption properties of the flame-retardant sample. Figure 3.12 shows a sample with a diameter of 30 mm and 60 mm that was cast by using the plastic mould. The samples were placed inside the impedance tube, and the Transfer Function Method (ASTM, ISO 10534-2) was used to figure out the properties of the sample in terms of sound absorption (BSWA Tech, 2022).

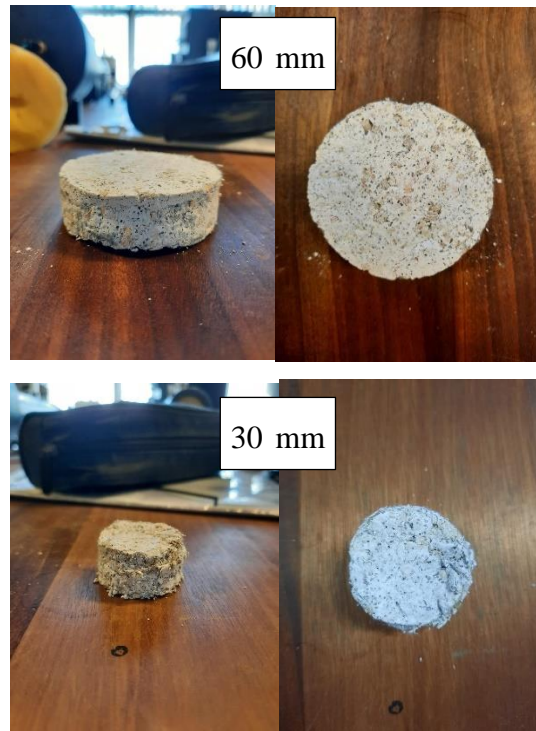


Figure 3.12: Two different diameters (60 mm and 30 mm) of the samples were cast.

BSWA Impedance Tube Measurement Systems manufactured by BSWA Technology Co., Ltd. were used in this research, as shown in Figure 3.13. When the sample was installed in the impedance tube, the loudspeaker in the tube emitted the quantified sound, and the microphones in the tube were used to detect the sound pressure level at a particular location along the tube. After that, the VA-Lab software measured the sound absorption of the sample based on the frequency response.

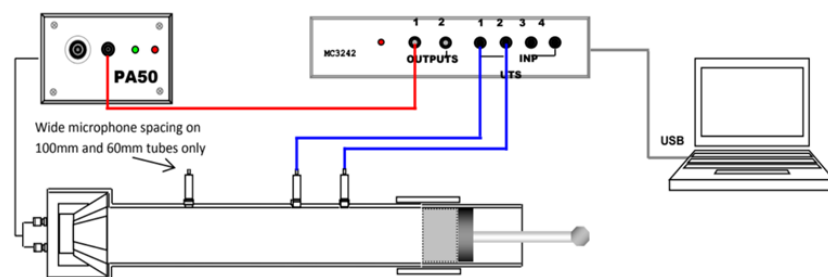


Figure 3.13: BSWA Impedance Tube Measurement Systems (Dokumen, 2023).

3.6.4 Three-point Flexural Test

This analysis examined the compression stress of the samples. A 300 mm × 30 mm × 40 mm sample was obtained from each of the prototype, and the machine used was the Shimadzu AGS-X with a 1 mm/min compression speed. The sample was supported over a span length of 150 mm while being compressed. Next, the compression was carried out until the sample was detached. Figures 3.14 and 3.15 represent the arrangement of the test.



Figure 3.14: The setup of the test.

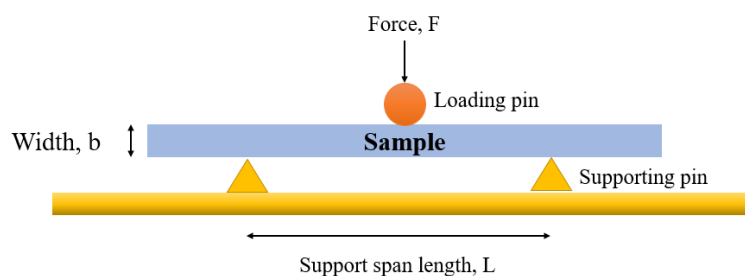


Figure 3.15: Illustration of the test.

This test was used to identify the testing samples' flexural strength and modulus. Flexural strength is the largest strength that the sample able to withstand, whereas the stress-strain deflection curve can determine the flexural

modulus. In simple words, the test can identify the amount of bending force the sample can resist. Equations 3.4 and 3.5 show the computation formulas for the flexural strength and flexural modulus, respectively.

Flexural strength calculation formula, σ_f (MPa):

$$\sigma_f = 3FL / 2bd^2 \quad (3.4)$$

Flexural modulus calculation formula, E_f (N/mm²):

$$E_f = L^3 m / 4bd^3 = \sigma_f / \varepsilon_f \quad (3.5)$$

where

σ_f = stress at the centre of the sample, MPa

ε_f = strain applied on the sample, mm/mm

E_f = flexural modulus of elasticity, MPa

F = load applied at a specific point, N

L = interval length between the supporting pins, mm

b = sample's width, mm

d = sample's thickness, mm

m = slope of the load-deflection curve, N/mm

3.7 Testing Methods for Best-Performing Fire-Retardant Board

3.7.1 1-hour Small-scale Fire Test

This test was similar to those in Section 3.6.1. It was conducted for one hour to analyse and compare the fire resistivity between the best-performing fire-retardant board and the commercial MgO board.

3.7.2 Density Measurement Test

The reason of conducting this test was to determine the density difference between the best-performing fire-retardant board and the commercial MgO board before and after carrying out the small-scale fire test. The calculation method was similar to that in Section 3.6.2.

3.8 Testing Methods for Fire Protection Duct

3.8.1 1-hour Small-scale Fire Test

This analysis evaluated the effectiveness of the fire protection duct in resisting the penetration of the hot flame as well as protecting the inner electrical cables for at least one hour. The test was conducted in a similar way with Section 3.6.1, whereby a 1000 °C flame from two Bunsen burners was sprayed on both sides of the fire protection duct for at least an hour. The temperature increment data of the fire protection duct for at least an hour. The temperature increment data was recorded by using a portable digital thermometer. Figure 3.16 represents the setup of the small-scale fire test.

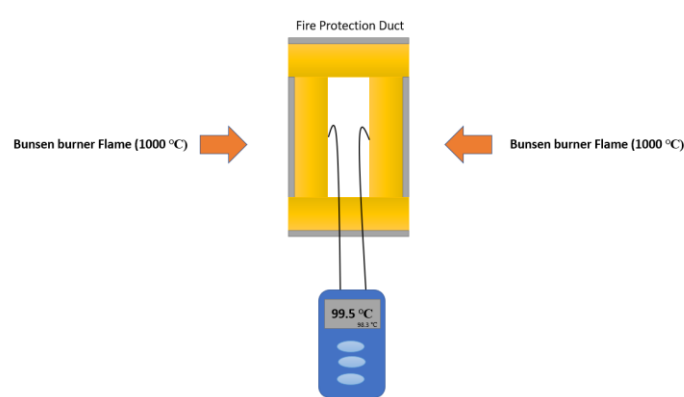


Figure 3.16: Schematic Diagram of a 1-hour Small-Scale Fire Test.

3.9 Summary

In short, a sequence of test analyses, such as the Bunsen burner test, static immersion, and adhesion strength tests, were performed to examine the resistance of fire, water, and adhesion strength properties of the samples (W-IB). Then, sample characterization tests such as the SEM test, the EDX test, the TGA test, and the FTIR test were carried out to examine the physical and thermal properties of the samples. Furthermore, a half-hour small-scale fire test, density measurement test, acoustic insulation test, and three-point flexural test were carried out among the prototypes to determine their performance in terms of fire resistivity, sound insulation, and mechanical strength. Furthermore, a 1-hour small-scale fire test and density measurement test were performed to analyse the characteristics of the best-performing fire-retardant board. Lastly, the fire protection duct was examined through 1-hour small-scale fire test to determine its temperature profile.

CHAPTER 4

RESULTS AND DISCUSSION

4.1 Introduction

After the testing methods for the W-IB, prototypes, best-performing fire-retardant board, and the fire protection duct were performed, the results for each testing method, with detailed analysis and discussion, were prepared in the following sessions.

4.2 Sample Characterization of Water-based Intumescent Binder

A series of testing methods for W-IB were conducted to inspect the performance of each flame-retardant additive, filler, binder, and material and to determine the best-performing compositions of the W-IB.

4.2.1 Bunsen Burner Test

This analysis inspected the performance of W-IB in resisting the high-pressure hot flame. By monitoring the char layer's thickness and the temperature profile during the test, the physical and chemical reactions of the W-IB can be evaluated.

A mild steel plate covered with four W-IB formulations (i.e., samples S1 to S4) was examined after a 30-minute Bunsen burner test. The critical temperature of the mild steel is 400 °C (Bilotta, Silva and Nigro, 2016). Thus, any samples that show a temperature near the critical temperature of the mild steel plate would qualify as failure compositions.

The temperature-to-time graph of the samples was plotted as shown in Figure 4.1. Following the test, all samples' equilibrium temperatures and char layer thicknesses were compiled in Table 4.1.

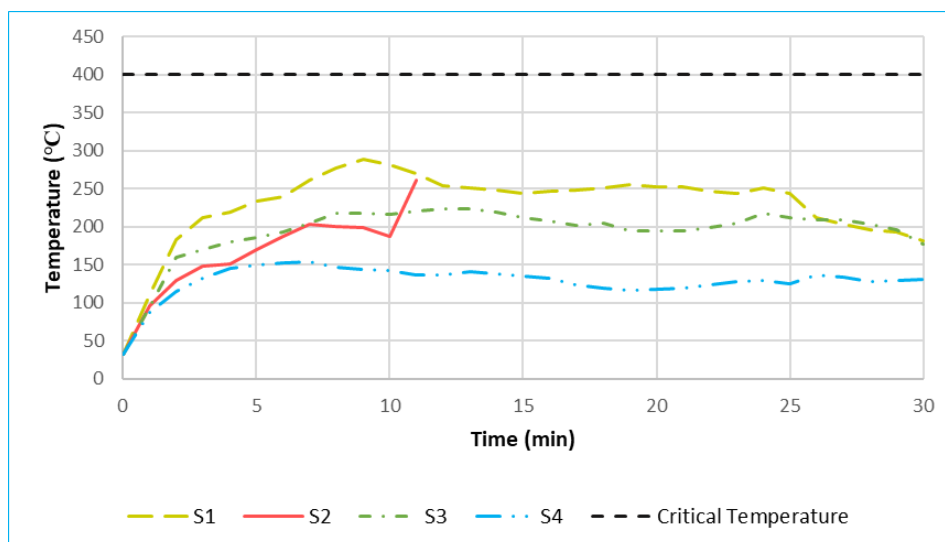


Figure 4.1: The Temperature Increment of All the Samples.

Table 4.1: Char layer thickness and equilibrium temperature of each sample.

Samples	Char Layer Thickness (± 0.1 mm)	Equilibrium Temperature of Sample ($^{\circ}\text{C}$)
S1	5 mm	250
S2	4 mm	200
S3	15 mm	209
S4	10 mm	128

From the temperature profiles displayed in Figure 4.1, all the W-IB exhibit similar temperature profile patterns in the first 2 minutes, which were below 250°C . Then, the temperatures started to alter for the next 8 minutes as the physical and chemical reactions began to happen when subjected to the high temperature. It was noticed that sample S1 began to swiftly raise the temperatures until 288°C . This might be due to the fact that the W-IB begins to lose its adhesion bonding with the mild steel plate, resulting in a rapid rise in temperature. At the same time, samples S4 begin to reduce the temperature slowly. This is because the EG found in sample S4 started to perform its function by reducing the burning rate and producing a thermally stable residue that acts as a protective barrier between the hot flame and the steel plate, as mentioned by Tomiak, et al., 2021. Thus, a constant temperature profile can be obtained.

The temperature profile of sample S2 rose to 261 °C and stopped at 11 minutes. This is due to the failure of the retort stand to clamp the sample S2 properly, which resulted in the sample falling off.

The temperature profiles of all the samples reached equilibrium between 12 and 25 minutes. Also, it was noticed that after 25 minutes, the temperatures of sample S1 started to fluctuate once more. S1 reduced the temperature significantly until 30 minutes. The equilibrium temperature of S4 of 128 °C was reviewed as having the lowest temperature profile among the other samples, thus showing the best result in terms of fire protection. The W-IB consists of the optimum ratio of additives, with the combinations of 2 wt. % Al₂O₃, 2 wt. % EG, and 3 wt. % CES promoting the best fire protective barrier, as mentioned by Jong, et al., 2019. Other than that, S1 exhibits the highest equilibrium temperature (250 °C). According to Xu, et al. (2015), it may be caused by the porosity and lightness that occurred in the char layer, which led to a decrease in adhesion between the char layer and the mild steel plate.

The purpose of measuring the char layer thickness after conducting the test was to evaluate each sample's ability to resist the propagation of the hot flame. The higher the thickness, the lesser the ability of the hot flame to propagate the W-IB, thus promoting a better fire resistance property. Throughout the test, sample S3 promotes the highest char layer expansion rate among the others. The reason is due to the high percentage of CES (18.5 wt. %) found in the sample. The decarbonation of CES increases the char layer expansion rate. When heated, it releases CO₂, to create calcium oxide, CaO. As a result of the protective char's restriction of heat, the underlying mild steel is preserved from fire damage (Yew and Sulong, 2012).

In short, samples S3 and S4 performed well throughout the test. S3 promoted the thickest char layer (15 mm) after 30 minutes of the Bunsen burner test, whereas S4 remained a constant and had the lowest temperature profile (128 °C) throughout the experiment.

4.2.2 Static Immersion Test

This analysis determined the W-IB's water resistivity. The W-IB can deteriorate for a variety of reasons, including humidity, the environment, human activities,

and others. Thus, it is crucial to assess the samples' water resistance using this method. Permeation and migration are the primary events that may occur during the immersion test. Figure 4.2 shows the weight change rate between the samples when immersed in water. The weight change percentage between the samples is shown in Table 4.2.

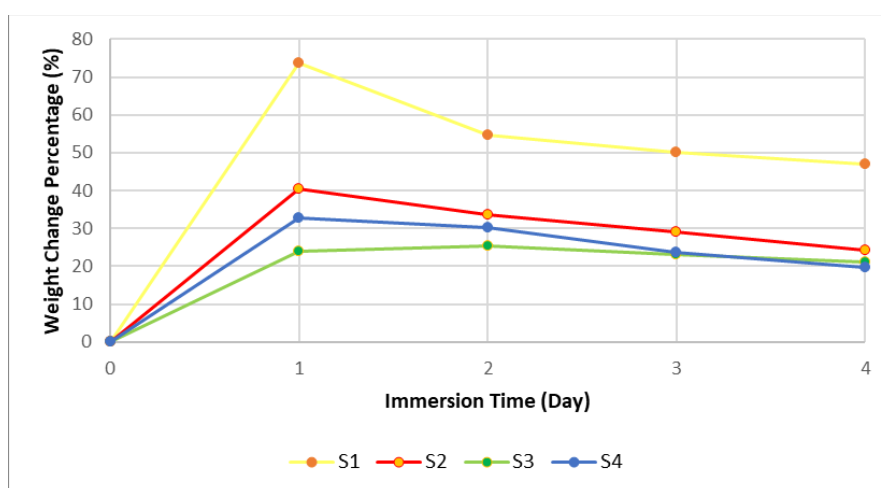


Figure 4.2: Weight Change Percentage of all the Samples.

Table 4.2: Weight Change Percentage among all the samples.

Samples	Weight Change Percentage (%)			
	First Day	Second Day	Third Day	Fourth Day
S1	73.66	54.68	50.19	47.12
S2	40.38	33.54	29.07	24.35
S3	23.92	25.25	22.99	21.14
S4	32.65	30.16	23.71	19.73

The water absorption rates of S1, S2, S3, and S4 during the first day were 73.66%, 40.38%, 23.92%, and 32.65%, respectively. From the results obtained, it can be seen that the permeation phase has been carried out, as the weight change percentage for all samples increased after the first day. This is primarily due to the fact that a higher amount of water is penetrated into the coated samples by the permeation phase than is transferred out by the migration process. Additionally, the ions and tiny molecules may permeate the sample's structure, causing weight growth.

Starting on the second day and continuing through the last day, the weight change percentage of most of the samples started to decrease. Among all the samples tested, sample S3 resumed the permeation phase on the second day, and it exhibited the least weight percentage changes over the course of the days. The reason is that the addition of CES filler with the additives and the binder exhibits a poor water absorption property, thus slowing down the water permeation and migration of the materials. This is more in accordance with the findings of the research study done by Yew, et al. in 2014. Therefore, the degree of permeation and migration processes throughout the testing can serve as a crucial piece of supporting evidence for the coating's water resistance property.

4.2.3 Adhesion Strength Test

This analysis evaluated the adhesion strength of each sample. The average adhesion strength of the samples is shown in Figure 4.3. The performance of the samples can be classified as poor or good. Samples 1, 3, and 4 showed an adhesion strength below 0.3 MPa, whereas sample 2 had the best performance and obtained the uppermost adhesion strength of 1.95 MPa.

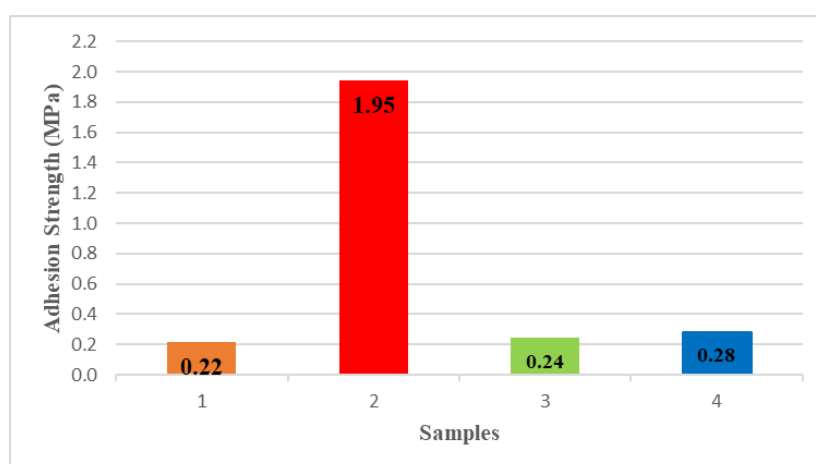


Figure 4.3: The Adhesion Strength of all the Samples.

The reason for having a good adhesion strength in sample S2 is due to the impact of the VAC binder and the oxide or hydroxide layer found on the steel substrate. The carbonyl group formed inside the VAC will react with the hydroxide layer of the substrate to generate a strong carbon-hydrogen (CH) bond. The addition of fillers to the composition further enhanced the relation

between the composition and the steel substrate (Netting, 2017 cited in Jong, et al., 2019). Therefore, the overall interactions between the VAC binder, additives, and steel substrate will have a significant effect on the adhesion strength properties (Santos, et al., 2000 cited in Jong, et al., 2019). Other than that, a strong electronegative atom (e.g., oxygen and hydrogen) combines to form a carbon-hydrogen bond. A VAC monomer would also generate hydrogen bonds with the steel substrate.

Furthermore, the compositions of Al_2O_3 and CES found in the sample S2 would also contribute to its highest adhesion ability. The interactions among the VAC binder and the hydroxide layer of the steel substrate, as well as the addition of Al_2O_3 and the CES, would distribute the stress uniformly. This is because mechanical stress, which occurs when there is a loss of adhesion between the compositions and the fillers, may increase the formation of voids in the matrix (Wang and Yang, 2010). Besides, the characteristics of the CES allowed the filler to perform well in reinforcement properties with the VAC binder (Xu, et al., 2016).

On the other hand, the performance of sample S4 is far below that of sample S2, although they have similar fillers (Al_2O_3 and CES). The reason is because the addition of EG found inside the composition may have some short-term outcomes in terms of fire protection properties and adhesion strength. According to Li, et al., 2021, EG promotes a great deal of the char layer formed during the combustion process that can resist the penetration of hot gas. However, the interaction between the char layer and the substrate is poor, which causes the char layer to be easily dismantled from the steel plate. Similar to this experiment, the addition of EG would cause a poor adhesion force because the interfacial compatibility between the EG and the substrate is very weak, which would then affect the quality of the mechanical properties. Thus, adding the EG into the compositions would decrease the adhesion strength property of the sample, even though well-performing fillers such as Al_2O_3 and CES were added. Apart from that, the adhesion strengths of samples S1 and S3, with 0.22 MPa and 0.24 MPa, respectively, did not possess a good adhesion strength property as the oxide layer might transform into the hydroxide layer under the effects of the moisture, which causes the change in morphology. Therefore, the choice of

an appropriate flame-retardant filler has a significant impact on the adhesive bonding between the compositions and the substrate. (Jong, et al., 2019).

4.2.4 Scanning Electron Microscopy (SEM) Analysis

This test analysed the surface morphology of the sample's char layer after it was subjected to the Bunsen burner flame gun for 30 minutes. Figure 4.4 shows the images of the entire sample's char layer after the Bunsen burner test. All the char layers were analysed under a magnification of 3000, which allowed the images to zoom in to 10 μm for accurate analysis.

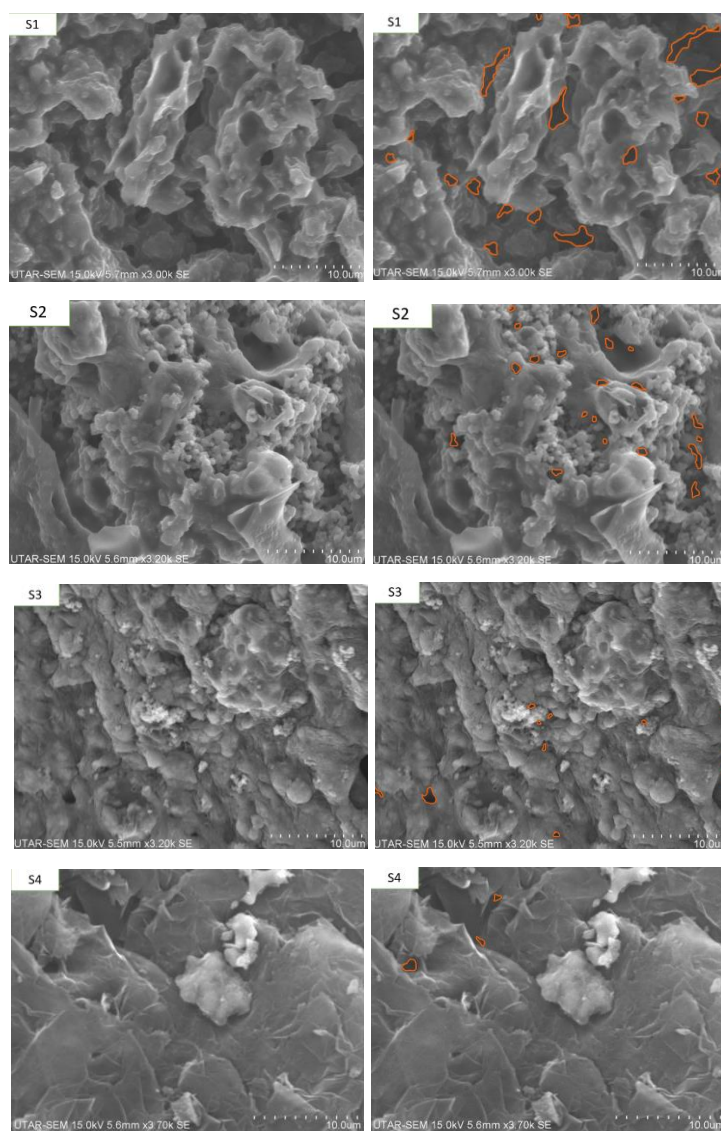


Figure 4.4: Surface Morphology of all Samples Char Layer.

The orange coloration shown in the SEM images in Figure 4.4 represented the pores found in the char layer. Samples S1 and S2 displayed larger and higher number of voids compared with samples S3 and S4. The reason is that when the sample was subjected to heat, these holes were created as a result of trapped gas found inside the blowing agent (Fredj, et al., 2008). Besides, the tiny holes were formed when the fire spread to the split lines on the W-IB structure (Beh, et al., 2019).

Additionally, sample S4's char layer was found to be denser and more compact as compared with other samples. A uniform foam structure can be seen and attached rigidly to the steel substrate after 30 minutes of exposure to the hot flame. Its stiff structure enhanced the distinctive qualities of the sample in fire protection.

In short, the makeup of the coating has an obvious impact on the fire protective performance that reveals the char layer's competence in flame resistivity (Toro, et al., 2007). It is important to keep in mind that the coating should be in a position to improve the intumescent binder's achievement in fire resistivity while choosing the specific formulation of the flame-retardant fillers (Santos, Santos and Toledo, 2000).

4.2.5 Energy-disperse X-ray (EDX) Spectroscopy Test

EDX was conducted to analyse the O/C ratio of the samples. In order to ascertain the antioxidant qualities of W-IB, the oxygen/carbon ratio is used in this research (Zia-ul-Mustafa, et al., 2015 cited in Jong, et al., 2019).

Free radicals, also known as reactive oxygen species, are volatile molecules with unpaired electrons. Samples with low O/C ratios display higher antioxidant properties. The reason is more free radicals are stabilised when they get an electron from the carbon bonds' resonance, which neutralises them. An antioxidant W-IB will function better in terms of fire protection and will stop fire from spreading to the steel plate beneath it. The oxygen/carbon ratio for each sample is shown in Figure 4.5.

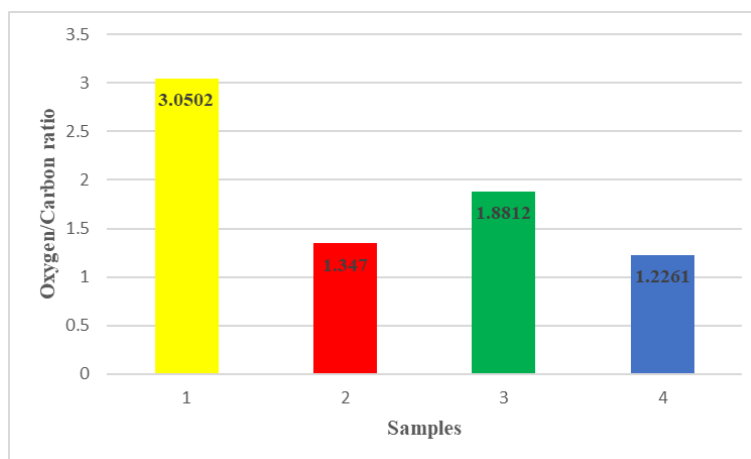


Figure 4.5: Oxygen/Carbon Ratio of all Samples.

From the outcomes obtained from Figure 4.5, the oxygen/carbon ratios of samples S1, S2, S3, and S4 are 3.0502, 1.3470, 1.8812, and 1.2261, respectively. It can be seen that sample S4 has the lowest ratio among the others. One can agree that a small oxygen/carbon ratio generates a low equilibrium temperature during the Bunsen burner test.

Throughout the analysed samples, phosphorus is the most abundant element found inside the compositions. The gaseous phase and the condensed phase are the two categories into which phosphorus can be divided. Phosphorus is utilised to suppress the flame in the gaseous phase, but when exposed to a high flame, it causes the char layer to grow larger in the condensed phase.

According to Md. Nasir, et al. (2018), the composition of the phosphorus will rise when the CaCO_3 is found in the W-IB. This viewpoint proved to be correct as a high level of phosphorus was found in sample S3 that contains CaCO_3 flame-retardant filler, as shown in Appendix A-3. The large amount of phosphorus also demonstrated good fire restriction, as the char layer thickness shown by S3 during the Bunsen burner test is the largest among the others.

On the other hand, W-IB with the inclusion of EG has demonstrated a negative response to the level of phosphorus. It is proven that the sample S4 that contains EG has the least amount of phosphorus, as shown in Appendix A-4. Even so, EG was found to be involved in thermal equilibrium properties. This is because, during the Bunsen burner test, sample S4 achieved the lowest

equilibrium temperature, which restricted a high temperature from penetrating through the W-IB.

Nevertheless, EDX's effectiveness in identifying carbon content varies. One could assert that carbon will always show up as an unavoidable contaminant in graphs. This is because the carbon peaks will be apparent because it is present on the vacuum chamber's walls. Additionally, the carbon contents can be formed through physical interactions or atmospheric diffusion at any step of processing. Therefore, to increase the precision of determining the carbon and oxygen levels in each sample, the sample plate should be carefully cleaned by plasma cleaning.

4.2.6 Thermogravimetric Analysis (TGA) Test

This test analysed the remaining weight percentage of the samples after they were heated to a high temperature (1000 °C). Its function is to observe the weight loss of the samples through degradative behaviour when heated. Each sample's TGA curve is depicted in Figure 4.6.

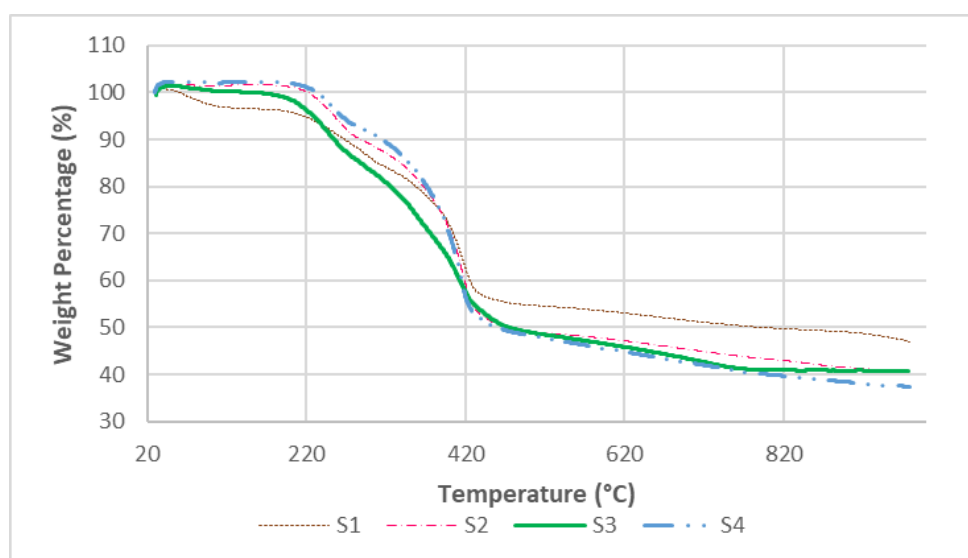


Figure 4.6: TGA Curve of each Prototype.

The result shows that the thermal decomposition of the samples occurred mainly between 220 °C and 420 °C. Each of the samples has a similar thermal degradation profile to the others, but some of them have a significant difference as shown. From 20 °C to 220 °C, most of the samples retained their initial

weight. However, sample S1 started to lose weight when the temperature reached 80 °C. When the temperature increased to 220 °C, samples S1 and S3 had a 5% initial weight loss. This is likely because of the release of moisture from the samples. While S2 and S4 were still able to maintain their initial weight without any degradation happening. From 220 °C to 320 °C, samples S1, S2, and S4 lost around 12 % of their initial weight, whereas 15 % of the initial weight of S3 was lost. Between 320 °C and 420 °C, approximately 30 % of initial weight loss occurred in all samples. However, between 420 °C and 520 °C, around 15 % to 20 % of initial weight loss was observed. This indicates that all the samples have started to reach their equilibrium state of degradation.

In short, the residue weights of samples S1, S2, S3, and S4 at 920 °C are 47.03 %, 40.94 %, 40.60 %, and 37.44 %, respectively. Sample S1 that contains $\text{Mg}(\text{OH})_2$ possesses more residue among the samples, showing the ability to enhance the thermal stability of the W-IB (Han, Guo, and Pan, 2022). However, samples S2, S3, and S4, with a residual weight of about 40%, also possess a good performance in enhancing the thermal stability of the intumescent binder. This is because some of the fillers (e.g., Al_2O_3 , CES, and EG) contain an interfacial hydrogen bond that restricts the spillover of materials from the W-IB (Nguyen, et al., 2023), as well as improving the anti-oxidation of the samples (Wang and Yang, 2012).

4.2.7 Fourier-transform Infrared (FTIR) Spectroscopy Test

This analysis looked into any possible modifications to molecular structure brought on by cross-linking between the mixtures. The detection of specific functional groups in the W-IB was investigated in the wavenumber spectrum between 500 c m^{-1} and 4000 c m^{-1} .

The analysed functional groups of all the samples were plotted as shown in Figure 4.7. The transform of the peak's position for each sample is presented in the figure. Samples 1 to 4 showed similar peaks and intensities. In the wavelength range of 3000 c m^{-1} to 3500 c m^{-1} , a broadband that consists of O–H stretch was observed due to the existence of intense intermolecular and intramolecular hydrogen bonds. The functional group found in this region can strengthen and increase the adhesive properties between the flame-retardant

materials and the binder as a consequence of the existence of hydrogen bonding (Yew, et al., 2018).

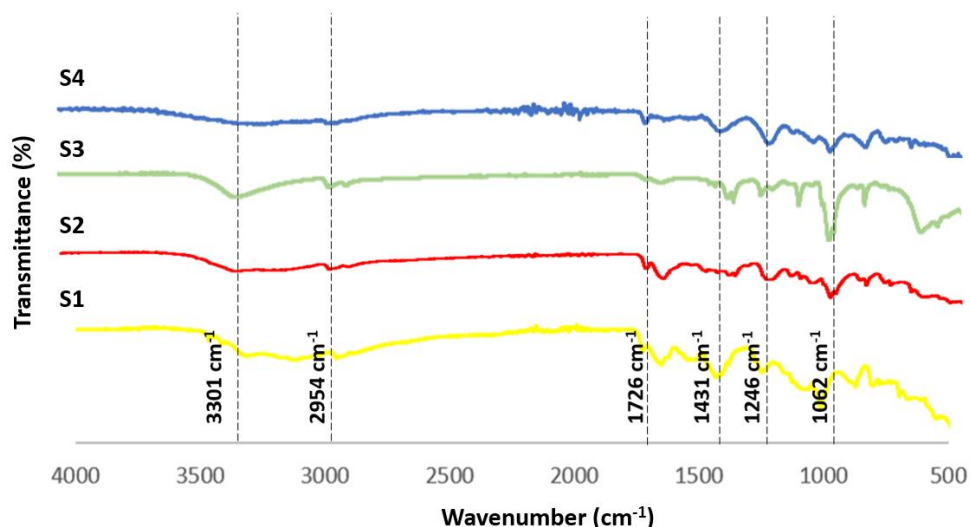


Figure 4.7: Functional Groups of all Samples.

The VAC binder, comprises of C–O (ester bond) and C=O (ester carbonyl) groups, was sensitive to the formation of hydrogen bonding. Due to the ease with which the –C–O vibration can link with other functional groups like the methyl group, CH₃, this transmittance is more sensitive to the formation of hydrogen bonds as compared with the –C=O transmittance. The methyl group, CH₃ stretch can be found at 2954 c m⁻¹. The result showed that samples S2 to S4 had a significant peak due to the addition of CES. The formulation of S1 with no addition of CES has a smaller peak as compared with the others.

In the region of 1062 c m⁻¹ to 1246 c m⁻¹, –C–O was observed, whereas C=O transmittance was found at the wavelength of 1726 c m⁻¹. Around 1431 c m⁻¹ transmittance, where the methane C–H bend can be discovered, is unleashed from the carbonization of the W-IB (Jong et al., 2019). The transmittance peak at 1382 c m⁻¹ represents the formation of the C–H bend of the methane group. The peak is difficult to see as it lies beneath strong methyl and methylene bands.

This study has established the critical role of hydrogen bonding in the adhesive characteristics of an intumescent binder. In order to validate the adhesion strength analysis in Section 4.2.3, this study can be used to explain the cross-linking between the W-IB.

4.3 Sample Characterization of Prototypes

A sample characterization of all the prototypes and the commercial MgO board has been conducted to analyse their fire protection performance when exposed to a 30-minute fire test. The temperature profile and the char layer generated by each prototype and the commercial MgO board provide a better understanding of how to determine the composition to fabricate the best-performing fire-retardant board. Besides, a density measurement of the prototypes and the commercial MgO board allowed the selection and fabrication of a light and durable fire-retardant board, which eases the installation of the fire protection duct.

4.3.1 Half-hour Small-scale Fire Test

This analysis examined the prototype's fire protection effectiveness. The temperature profiles of the prototypes and the commercial MgO board were plotted, as shown in Figure 4.8. The outcome shows that the commercial MgO board had a significant temperature increment in the first 5 minutes. After it reached the maximum temperature of 385 °C, the temperature started to drop and ceased at 7 minutes. It was because the MgO board was broken due to its poor integrity when exposed to a high temperature flame and caused the temperature measuring sensor dropped down. Thus, one can be deduced that the commercial MgO board has a low ability to resist a high temperature. Besides, the temperature responses of prototypes P1 and P2 were similar for the first 5 minutes, which showed a higher temperature profile as compared with P3 and P4. In the first 5 minutes, P1 and P2 rose significantly towards 200 °C. P2 then increased gradually from 5 minutes to 7 minutes until it reached 229 °C. After that, it showed a steady but fluctuating temperature profile throughout the test. The reason might be because the chemical and physical reactions started to happen inside the intumescent binder when exposed to the hot flame. At the same time, P1 kept increasing significantly until 222 °C at 9 minutes and decreased gradually until 171 °C at 30 minutes.

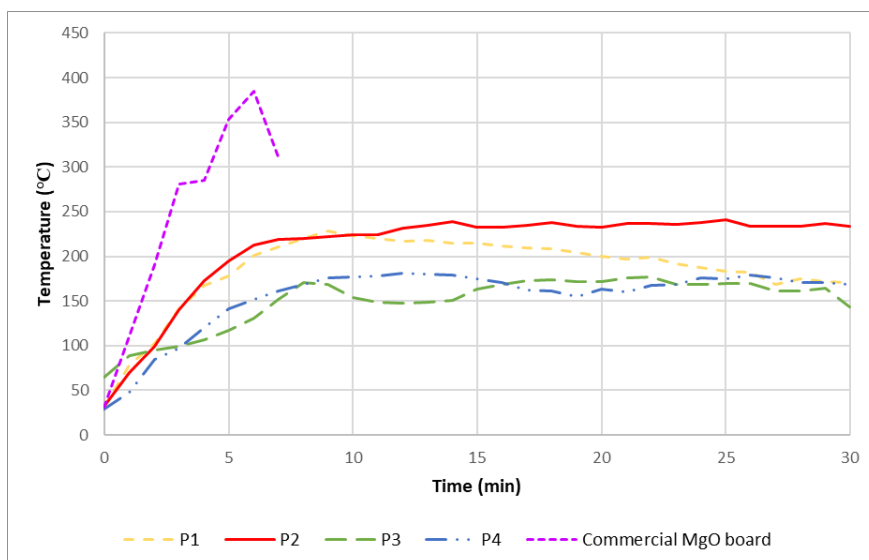


Figure 4.8: Temperature Profiles of the Prototypes and the commercial MgO board.

Prototypes P3 and P4 showed a lower temperature profile throughout the test. The responses of P3 and P4 were similar in the first 3 minutes, which were below 100 °C. Then, P4 started to rise rapidly until 176 °C at 9 minutes. It then remained that temperature until 15 minutes and started to drop from 175 °C to 155 °C at the end of 19 minutes. After that, P4 gradually increased the temperature again, showed a slight drop-off at 27 minutes, and finally reached 168 °C at 30 minutes.

P3 performed well in the test as it showed the lowest temperature profile compared to others. P3 rose significantly after the first 5 minutes and started to reduce at 10 minutes. Later, it increased gradually until it reached 173 °C and maintained the temperature from 15 to 23 minutes. Lastly, the temperature profile started to reduce and finally reached 143 °C at 30 minutes. Throughout the test, it was noticed that the increment of the temperature profile of P3 was the slowest among the prototypes. Therefore, it can be deduced that P3 performed the best in fire resistivity due to the lowest temperature profile. Besides, P4 also performed well as it possesses a low temperature profile and generated the thickest char layer among the others, as shown in Figure 4.9. This may be due to the presence of EG, which showed a sensitive response to the high temperature.

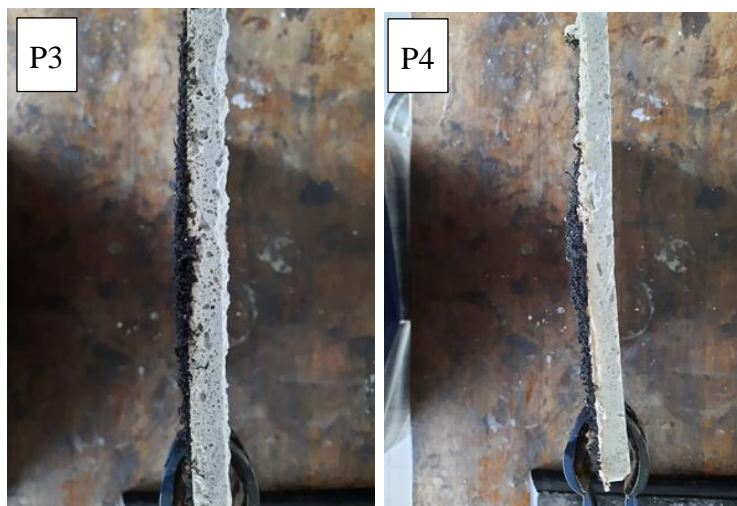


Figure 4.9: P4 showed a Thicker Char Layer than P3.

4.3.2 Density Measurement Test

Table 4.3 represents the change in density of the prototypes and the commercial MgO board pre and post of the 30-minute small-scale fire test. Figure 4.10 illustrates the weight loss percentage of the testing materials. From the results obtained, it was noticed that prototype P4 had the lowest weight loss (5.56 %) in the measurement. Although it possesses a high density among the prototypes, in which the high weight might be due to the addition of EG and PET textile fibres, the performances from the previous tests have proved that P4 can perform well in terms of fire protection, water repulsion, sample characterization (e.g., SEM analysis and EDX test), etc. Thus, the composition of the prototype P4 can be used to cast the best-performing fire-retardant board. On the other hands, the commercial MgO board possesses the highest density before and after carrying out the test. It also showed a high percentage of weight loss (20 %).

Table 4.3: Density Changes of all Prototypes and the commercial MgO board.

Prototypes	Density (kg/m ³)		
	Before Testing	After Testing	Weight Loss Percentage (%)
Commercial MgO board	1097.3900	877.9100	20.00
P1	511.5646	402.7211	21.28

P2	549.6599	440.8163	19.80
P3	609.5238	527.8912	13.39
P4	685.7143	647.6190	5.56

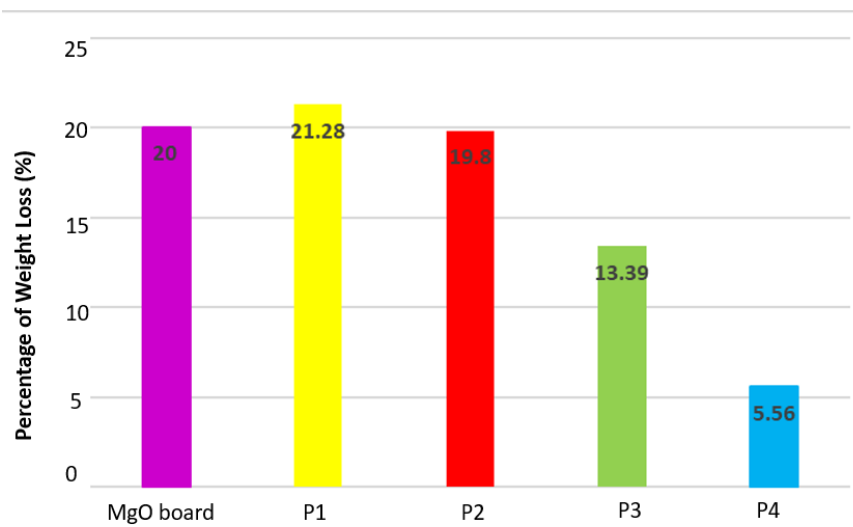


Figure 4.10: Weight Loss Percentage of the Prototypes and the Commercial MgO board.

4.3.3 Sound Insulation Test

A sound insulation test was performed to determine and analyse the sound absorption coefficient of the flame-retardant sample.

In general, the sound absorption coefficient of common materials used in the market lies between 0 and 1. For example, gypsum board that is used to resist fire penetration has a sound absorption coefficient of 0.1 (Commercial Acoustics, 2016). Thus, the flame-retardant sample prepared must exceed a 0.1 coefficient to enhance the sound insulation performance.

Table 4.4: The Average Sound Absorption Coefficient of the Sample Prototype.

Sample prototype	Frequency (Hz)						Average AC
	125	250	500	1000	2000	4000	
	Absorption Coefficient (AC)						
	0.15	0.12	0.12	0.15	0.30	0.41	0.2083

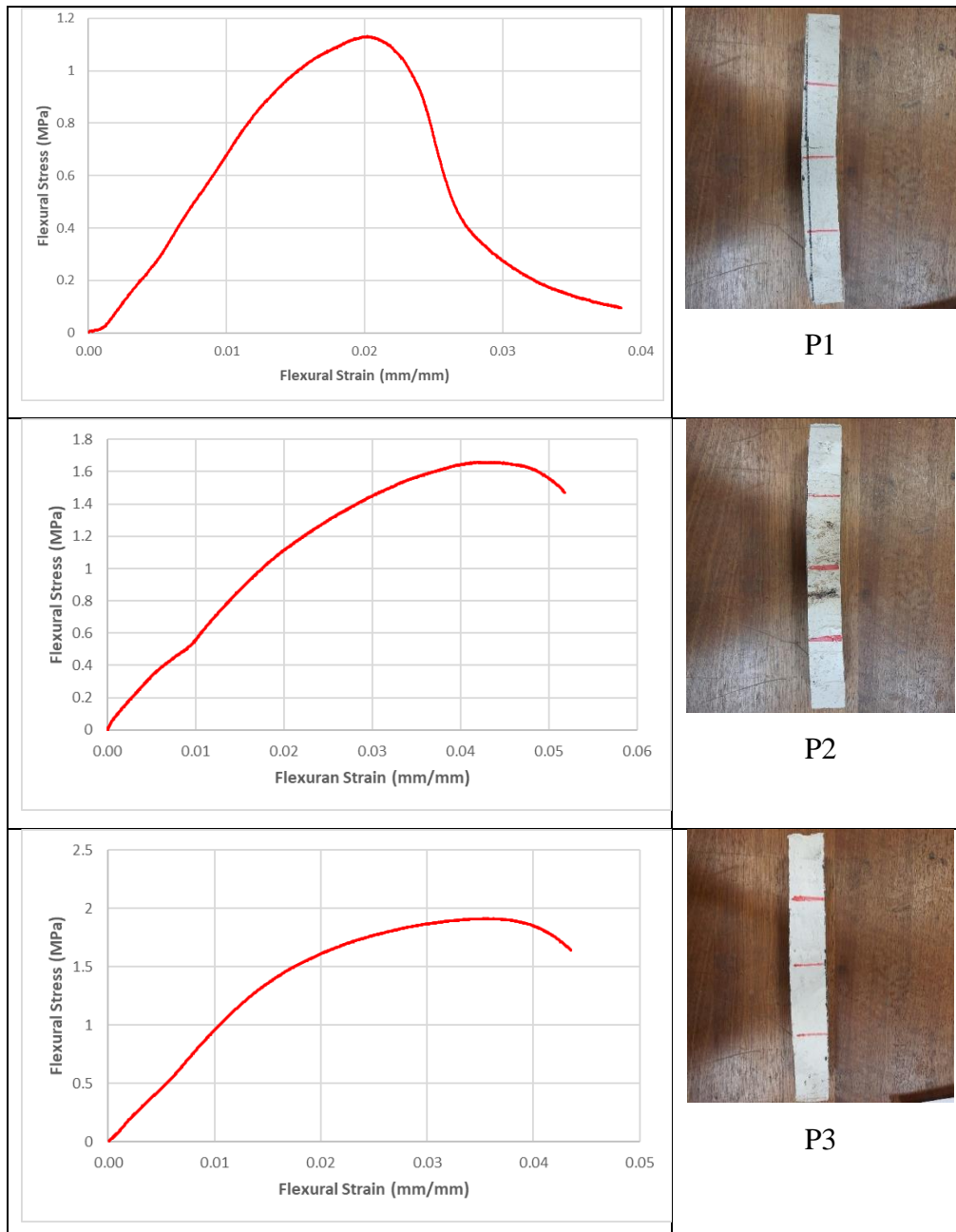
From the result obtained, it can be noticed that the ability of the sample prototype in absorbing a sound is higher than that of the commercial gypsum board, which is 0.21. Thus, the flame-retardant material prepared with the inclusion of Al_2O_3 , CES, EG, and VAC binder achieved a higher acoustic standard than the gypsum board. Besides, one should be aware that the sound absorption coefficient is not only subjective to the materials themselves but also depends on environmental factors (e.g., room temperature, humidity, atmospheric pressure). Therefore, soft materials have a higher ability to absorb sound than hard or rigid materials.

4.3.4 Three-point Flexural Test

The general purpose of the fire-retardant board or fire protection duct is to resist thermal degradation. However, the board tends to bend inwardly when the exposure time to the hot flame is large. This is because the non-uniform distribution of the high temperature will create an unbalanced stress inside the board, thus causing the ease of the high temperature to penetrate the board. Therefore, this test was performed to analyse the bending strength of the board in order to calculate its flexural strength and flexural modulus.

Flexural strength is measured and calculated to determine the maximum stress the outer fibre can withstand. In other words, high flexural strength properties indicate high toughness and high resistivity to external impacts. Besides, flexural modulus characterises the stiffness of the samples. For example, a high value of flexural modulus indicates that the sample has a high resistance to bending. Figure 4.11 shows the maximum load that each prototype sample can withstand. From the results obtained, the maximum force that each prototype can withstand is in linear order (i.e., $F_{P4} > F_{P3} > F_{P2} > F_{P1}$),

showing that prototype P1 has the lowest ability to withstand a high load, whereas prototype P4 can withstand the highest external impact among the others before the first crack. Thus, prototype P4 possesses the highest flexural stress and ductility among the prototypes.



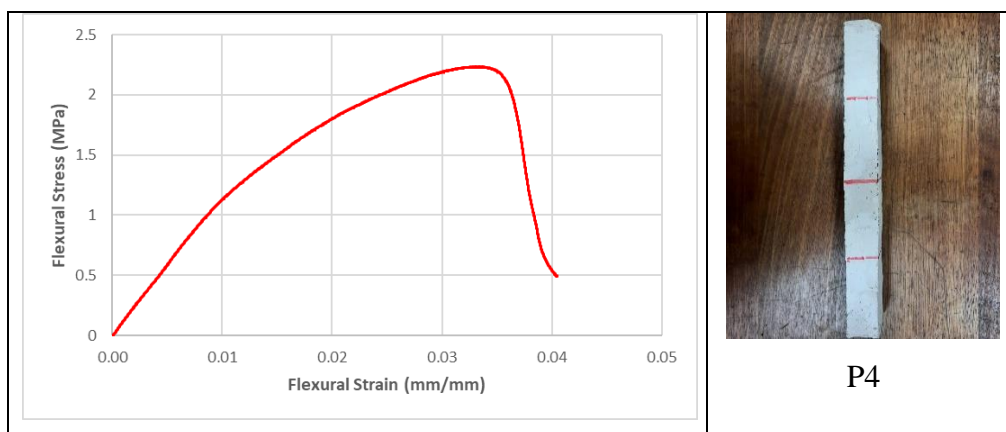


Figure 4.11: The stress-strain curve and the prototypes after conducting the test.

Table 4.5 indicates the flexural stress and flexural modulus calculated for each prototype sample. The results showed that the flexural stress and flexural modulus are in linear order (i.e., $F_{P4} > F_{P3} > F_{P2} > F_{P1}$). Meaning that prototype P4 possesses the highest flexural stress and flexural modulus, whereas prototype P1 has the lowest flexural stress and flexural modulus. It is revealed that prototype P4 has the highest stress of 2.2313 MPa and the highest modulus of 53.55 N/mm². It thus proves that P4 can receive the highest impact of stress and resist bending. The higher the flexural modulus, the more resistance the prototype has to bend.

Table 4.5: Flexural Stress and Flexural Modulus of the prototypes.

Samples	Flexural Stress, σ_f (MPa)	Flexural Modulus, E_f (N/mm²)
P1	1.1323	26.23
P2	1.6598	26.37
P3	1.9136	44.76
P4	2.2313	53.55

Prototype P3 shows a high flexural stress and modulus of 1.9136 MPa and 44.76 N/mm², respectively. The properties possessed by P3 are similar to those of P4, which means that it has the ability to withstand high impact loads and high bending stresses. Besides, P2 shows a low flexural stress of 1.6598

MPa with a flexural modulus of 26.37 N/mm², and P1 shows a low flexural stress of 1.1323 MPa with a flexural modulus of 26.23 N/mm². This indicates that both P1 and P2 are very brittle and tend to bend easily when a force is applied. Furthermore, the high equilibrium temperature shown by P1 and P2 in Section 4.3.1 proves that the high temperature will cause the material to become flexible and reduce its flexural modulus. Therefore, prototype P4 possesses the most suitable materials to construct the fire protection duct, as it can withstand the highest impact load and bending.

4.4 Sample Characterization of Best-Performing Fire-Retardant Board

4.4.1 1-hour Small-scale Fire Test

This analysis determined the fire resistivity of the best-performing fire-retardant board (P4) with the commercial MgO board. The temperature profile of each testing sample in function of time is tabulated in Figure 4.12. From the results obtained, prototype P4 and the commercial MgO board showed a similar temperature profile during the first 20 minutes. Both of them increased the temperature rapidly from 28 °C to 76 °C and then rose gradually until reaching 110 °C in 20 minutes. After that, they showed a significant difference in terms of fire resistivity. The commercial MgO board rose again significantly from 20 minutes to 30 minutes, reaching a temperature of around 200 °C. It then returned to rising normally for another 30 minutes until the end of the test. At 60 minutes, the commercial MgO board reached nearly 300 °C. On the other hand, prototype P4 showed a comparatively lower temperature profile throughout the test. It starts to show an equilibrium temperature of 100 °C from 10 minutes to 50 minutes. This is because the inclusion of good thermal insulation, vermiculite, helps to disperse the heat when exposed to the hot flame. After that, P4 increased its temperature gradually and reached 140 °C in 60 minutes. From this observation, prototype P4 showed a significantly better performance in terms of fire resistivity than the commercial MgO board. Therefore, P4 can be classified as the best fire-retardant prototype to resist the penetration of high temperatures and maintain a low equilibrium temperature throughout the fire test.

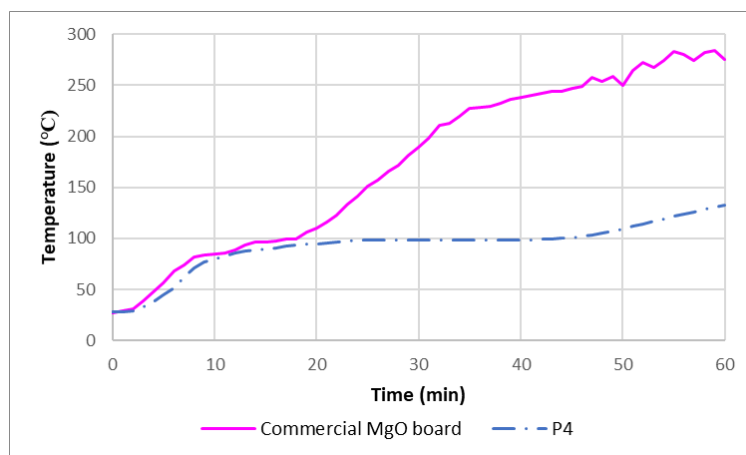


Figure 4.12: Temperature Profiles of Prototype P4 and the Commercial MgO board.

4.4.2 Density Measurement Test

Table 4.6 shows the density of the commercial MgO board with the prototype P4 pre and post of the 1-hour small-scale fire test. Figure 4.13 illustrates the weight loss percentage of both the MgO board and P4. From the results obtained, prototype P4 has a slightly higher density than the commercial MgO board before and after the test. This might be due to the addition of EG and some PET fibres, which increase the weight of the prototype. However, prototype P4 showed a relatively lower percentage of weight loss (17 %) after being exposed to the hot gas, as compared with the weight loss percentage of 37.60 % from the commercial MgO board. This test has proved that the integrity of the prototype P4 can be maintained without losing much of its density after being exposed to a one-hour fire. Thus, P4 has a better capability to protect the items (e.g., electrical cables) stored behind it without causing major damage.

Table 4.6: Density changes of Prototype P4 and the Commercial MgO Board.

Prototypes	Density (kg/m ³)		
	Before Testing	After Testing	Weight Loss Percentage (%)
Commercial MgO board	1097.39	684.77	37.60
P4	1045.39	867.67	17.00

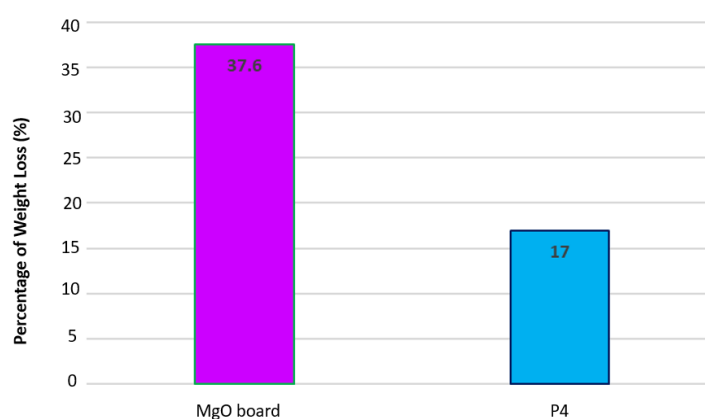


Figure 4.13: Weight Loss Percentage of Prototype P4 and the Commercial MgO board.

4.5 Sample Characterization of Fire Protection Duct

4.5.1 1-hour Small-scale Fire Test

This analysis determined the temperature profile of the fire protection duct after exposure to a 1-hour small-scale fire. Two thermocouples were attached to both sides of the duct, with the label T1 on the right side of the duct and T2 on the left side, as shown in Figure 4.14.

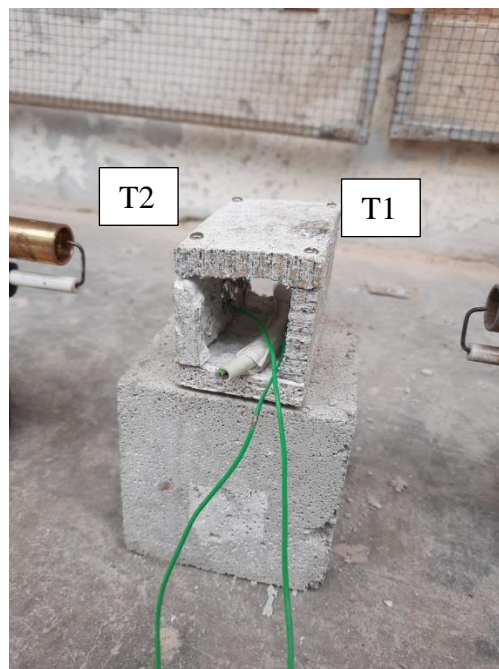


Figure 4.14: Both sides (T1 and T2) of the fire protection duct were exposed to fire for 1 hour.

Figure 4.15 shows the temperature increments of T1 and T2 throughout the test. From the results obtained, the temperature profiles of T1 and T2 showed similar results as the fire protection duct was assembled using prototype P4. In the first 2 minutes, T1 and T2 exhibit similar temperature increments to 120 °C. Then, T1 increased gradually until reaching 155 °C at 17 minutes before dropping down. On the other hand, T2 exhibits a higher temperature for the first 10 minutes. This might be due to the influence of wind direction, as the test was conducted outdoors. After that, the temperature of T2 dropped significantly for 26 minutes. This is because the Bunsen burner flame gun was running out of gas. Then, it rose up again until it reached around 180 °C before it started to drop down. From 40 minutes to 60 minutes, the temperature profiles of both T1 and T2 showed similar patterns. This test showed that a low temperature profile (e.g., 180 °C and 130 °C) can be maintained by the fire protection duct when exposed to the hot flame. Besides, the conditions of the electrical cable remain unchanged after the 1-hour fire test, as shown in Appendix B-6. Therefore, one can deduce that the fire protection duct has the ability to protect the electrical cable by providing a low temperature and maintaining the conditions of the cable.

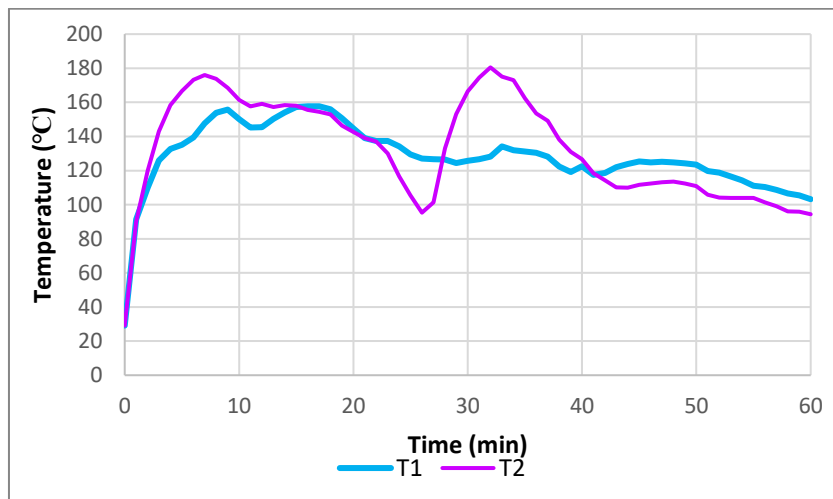


Figure 4.15: Temperature Profile of right (T1) and left (T2) sides of the fire protection duct.

4.6 Cost Analysis of Fire-Retardant Board

One of the purposes of developing a non-halogenated W-IB is due to its low-cost properties. In this research, a 175 mm × 175 mm × 30 mm fire-retardant board was used to construct an 85 mm × 50 mm × 60 mm small-scale fire protection duct. Table 4.7 shows the overall cost of the fire-retardant board required. All the market prices were referred from a Chinese manufacturer, Made-in-China.com. With a total weight of 800 g, the cost required to fabricate a fire-retardant board is RM 7.19.

Table 4.7: The Price required to cast a 0.8 kg, 175 mm x 175 mm x 30 mm Fire-retardant board.

Flame-retardant materials	Compositions (g)	Cost (RM/Compositions)	*Remark
APP	240	1.60	Minimum purchase of 1000 kg, with RM 6.66/kg
PER	80	0.53	Minimum purchase of 1 kg, with RM 6.66/kg

MEL	80	0.50	Minimum purchase 5 tons, with RM 6.17/kg
EG	16	0.15	Minimum purchase 1 kg, with RM 9.32/kg
Al ₂ O ₃	16	0.58	
CES	24	0.34	
TiO ₂	24	0.19	
VAC	320	2.11	Minimum purchase 15 tons, with RM 6.66/kg
Vermiculite	0.8L	1.19	
Total Price		7.19	

According to Rise Home Design Inc. (2023), the market price of the commercial MgO board costs USD 1.60 per square foot (RM 7.10 per 92 903 mm²). If compared with the dimensions of the fire-retardant board used in this research, the MgO board costs about RM 10.38. Thus, it is more expensive than the fire-retardant board (e.g., RM 7.19). Additionally, the commercial MgO board's temperature profile and weight loss percentage were greater than those of the prototype P4 as indicated in Sections 4.4.1 and 4.4.2. Thus, it can be demonstrated that the W-IB is significantly superior to the MgO board when used in passive fire protection system.

4.7 Summary

The testing results of the W-IB, prototypes, the best-performing prototype, and the fire protection duct were summarised as shown in Tables 4.8, 4.9, 4.10, and 4.11, respectively.

Table 4.8: Summary of the W-IB testing results.

Samples	S1	S2	S3	S4
Bunsen burner test	Highest equilibrium temperature with a thin char layer	Higher equilibrium temperature with the thinnest char layer	High equilibrium temperature with the thickest char layer	Lowest equilibrium temperature with a thick char layer
Static immersion test	Worst water resistance	Good water resistance	Best water resistance	Better water resistance
Adhesion strength test	Lowest adhesion strength	Highest adhesion strength	Lower adhesion strength	Low adhesion strength
SEM test	Worst surface profile	Good surface profile	Better surface profile	Best surface profile
EDX test	Highest O/C ratio	Low O/C ratio	High O/C ratio	Lowest O/C ratio
TGA test	Highest residue weight	Higher residue weight	Slightly higher residue weight	High residue weight
FTIR test	Presence peaks: –OH, CO, CH ₃ ,	Presence peaks: –OH, CO, CH ₃ ,	Presence peaks: –OH, CO, CH ₃ ,	Presence peaks: –OH, CO, CH ₃ ,

	C=O, C-H bend	C=O, C-H bend	C=O, C-H bend	C=O, C-H bend
--	------------------	------------------	------------------	------------------

Table 4.9: Summary of the Prototypes' testing results.

Samples	MgO board	P1	P2	P3	P4
Half-hour small-scale fire test	Highest temperature profile	High temperature profile	Higher temperature profile	Lowest temperature profile	Low temperature profile
Density measurement test	Slightly higher weight loss %	Highest weight loss %	High weight loss %	Low weight loss %	Lowest weight loss %
Sound insulation test	-	0.21 sound absorption coefficient	0.21 sound absorption coefficient	0.21 sound absorption coefficient	0.21 sound absorption coefficient
Three-point flexural test	-	Lowest Flexural Stress and Flexural Modulus	Low Flexural Stress and Flexural Modulus	High Flexural Stress and Flexural Modulus	Highest Flexural Stress and Flexural Modulus

Table 4.10: Summary of the Best-performing Fire-retardant board testing results.

Samples	MgO board	P4
1-hour small-scale fire test	High-temperature profile	Low-temperature profile
Density measurement test	High weight loss %	Low weight loss %

Table 4.11: Summary of the Fire protection duct's testing result.

Sample	Fire protection duct
1-hour small-scale fire test	Low-temperature profile without damaging the electrical cable

CHAPTER 5

CONCLUSIONS AND RECOMMENDATIONS

5.1 Conclusions

W-IB, coupled with different compositions of the additive, were examined and evaluated through fire resistance testing (e.g., Bunsen burner test), chemical testing (e.g., static immersion test), mechanical testing (e.g., adhesion strength test), physical testing (e.g., SEM/EDX test, FTIR test), and thermal testing (e.g., TGA test). Four different compositions of the fire-retardant board prototypes were analysed by a half-hour small-scale fire test, a density measurement test, a sound insulation, and a three-point flexural tests. Furthermore, the leading-performing composition was chosen to cast a 175 mm x 175 mm x 30 mm best-performing fire-retardant board with a density of 1045.39 kg/m³ to perform a 1-hour small-scale fire test. Lastly, the fire protection duct was assembled using the best-performing fire-retardant board.

The summary of each test was concluded as below:

Sample Characterization of Water-Based Intumescent Binder

a) Fire Resistance Test (i.e., Bunsen burner test)

Sample S3 promotes the highest char layer expansion rate due to the high percentage of CES (18.5 wt. %) that releases CO₂ to create CaO. Besides, sample S4 had the lowest temperature profile (128 °C) due to the combinations of 2 wt. % Al₂O₃, 2 wt. % EG, and 3 wt. % CES, promoting the best fire protective barrier.

b) Chemical Test (i.e., Static immersion test)

Sample S3 exhibited the least weight percentage changes due to the inclusion of CES filler with the flame-retardant additives and the binder exhibits a poor water absorption property, thus slowing down the water permeation and migration of the materials.

c) Mechanical Test (i.e., Adhesion strength test)

Sample S2 has a good adhesion strength because the carbonyl group formed inside the VAC will react with the hydroxide layer of the substrate to form a strong carbon-hydrogen (CH) bond. The addition of Al_2O_3 and the CES also distribute the stress uniformly. On the other hand, sample S4 has a performance far below that of S2. This is due to the fact that the addition of EG would cause a poor adhesion force between the W-IB and the underneath steel substrate.

d) Physical Tests (i.e., SEM/EDX test, FTIR test)

In SEM analysis, sample S4 was found to be denser and more compact, as a uniform foam structure can be seen and is attached rigidly to the steel substrate.

Based on the results obtained in EDX test, W-IB with the inclusion of CaCO_3 promotes a high volume of phosphorus, and the phosphorus will generate a good fire restriction. On the other hand, S4, with the least amount of phosphorus, possesses the lowest oxygen/carbon ratio, demonstrating that the low volume of phosphorus would allow the W-IB to exhibit good antioxidant properties.

In FTIR test, a broadband that consists of O–H stretch found between the wavelengths of 3000 c m^{-1} and 3500 c m^{-1} has the existence of intense intermolecular and intramolecular hydrogen bonds, which would strengthen and increase the adhesive properties between the flame-retardant materials and the binder due to the existence of hydrogen bonding.

e) Thermal Test (i.e., TGA test)

This test shows that sample S1 with the inclusion of $\text{Mg}(\text{OH})_2$ possesses more residue among the samples. However, samples S2, S3, and S4, with a residual weight of about 40%, also possess a good performance in enhancing the thermal stability of the intumescent binder.

Sample Characterization of Prototypes

f) Half-hour Small-scale Fire Test

This test showed that prototype P3 has the lowest temperature profile, even after 30 minutes of heating. Besides, P4 also performed well as it possesses a low temperature profile and generated the thickest char layer among the others.

g) Density Measurement Test

This test reviewed the change in density among the prototypes pre and post of the 30-minute small-scale fire test. From the results obtained, prototype P4 had the lowest weight loss (5.56 %) in the measurement.

h) Sound Insulation Test

From the result obtained, the ability of the sample prototype to absorb a sound is higher than that of the commercial gypsum board (e.g., 0.1), which is 0.21. Thus, the formulated W-IB possesses a higher sound absorption ability than commercial gypsum board.

i) Three-point flexural Test

Prototype P4 has the highest flexural stress of 2.2313 MPa and the highest flexural modulus of 53.55 N/mm². It thus proves that P4 can receive the highest impact of stress and resist bending. The higher the flexural modulus, the more resistance the prototype has to bend.

Sample Characterization of Best-Performing Fire-Retardant Board

j) 1-hour Small-scale Fire Test

The results revealed that prototype P4 had a lower temperature profile (100 °C) throughout the 1-hour fire test. However, the commercial MgO board has a comparatively higher temperature profile, with a temperature closer to 300 °C at the end of the test.

k) Density Measurement Test

Prototype P4 has revealed a lower weight loss percentage (17 %) as compared with the commercial MgO board (37.6 %).

Sample Characterization of Fire Protection Duct

The result revealed that both T1 and T2 maintained the temperature below 200 °C with the formation of thick char layers to resist the penetration of hot flame. Other than that, the conditions of the electrical cable remain unchanged after the 1-hour fire test. Therefore, the fire protection duct has passed the test to protect the electrical cables during the fire outbreak.

5.2 Recommendations for future work

After conducting all the sample characterizations for this research, there are various suggestions that can be made to enhance the outcomes obtained and improve the performance of the fire-retardant board as well as the fire protection duct. One of the possible recommendations from this research is to further improve the formulation or composition of the W-IB as well as the fire-retardant board. A high-performance flame-retardant material should be purchased to achieve the desired or better results for the sample characterizations.

When casting the 175 mm x 175 mm x 30 mm best-performing fire-retardant board using the cast-iron mould, it is recommended to remove the prototype from the mould after the shape is formed and heat up the prototype in the furnace at 70 °C for at least 2 days. This progress can speed up the drying speed of the prototype. Besides, avoid using too much water in the composition when casting the fire-retardant board. This is because the excess water may leak from the cast iron mould, causing shrinkage of the prototype as well as loosening its compatibility.

Last but not least, it is fully recommended to design and fabricate a real-life, full-scale fire protection duct to determine the workability of the W-IB in terms of fire protection in real-life environments. Some industrial standards (SIRIM Fire Test) should also be followed to convince and prove the

effectiveness of the halogen-free flame-retardant materials in resisting fire propagation.

REFERENCES

- Abd El-Wahab, H., 2015. Synthesis and characterisation of the flame-retardant properties and corrosion resistance of Schiff's base compounds incorporated into organic coating. *Pigment and Resin Technology*, [online] Available at: <https://www.researchgate.net/publication/276441720_Synthesis_and_characterisation_of_the_flame_retardant_properties_and_corrosion_resistance_of_Schiff's_base_compounds_incorporated_into_organic_coating> [Accessed 31 March 2023].
- American Elements, 2023. *Ammonium Polyphosphate*. [online] Available at: <<https://www.americanelements.com/ammonium-polyphosphate-68333-79-9>> [Accessed 1 August 2022].
- Ariyanayagam, A.D. and Mahendran, M., 2017. Fire tests of non-load bearing light gauge steel frame walls lined with calcium silicate boards and gypsum plasterboards. *Thin-Walled Structures*, [e-journal] 115, pp.86-99. <http://dx.doi.org/10.1016/j.tws.2017.02.005>.
- Awogbemi, O., Inambao, F. and Onuh, E., 2020. Modification and characterization of chicken eggshell for possible catalytic applications. *Heliyon*, [e-journal] 6(10). <https://doi.org/10.1016/j.heliyon.2020.e05283>.
- Beh, J.H., Yew, M.C., Saw, L.H. and Yew, M.K., 2020. Fire resistance and mechanical properties of intumescent coating using novel BioAsh for steel. *Coatings*, [e-journal] 10(11). <https://doi.org/10.3390/coatings10111117>.
- Beh, J.H., Yew, M.C., Yew, M.K. and Saw, L.H., 2019. Fire protection performance and thermal behaviour of thin film intumescent coating. *Coatings*, [e-journal] 9(8), 483. <https://doi.org/10.3390/coatings9080483>.
- Benarx, 2022. *Epoxy cable tray*. [online] Available at: <<https://www.benarx.com/products/fire-series/epoxy-cable-tray/>> [Accessed 28 June 2022].
- Bilotta, A., Silva, D.D. and Nigro, E., 2016. Tests on intumescent paints for fire protection of existing steel structures. *Construction and Building Materials*, [e-journal] 121, pp.410-422. <http://dx.doi.org/10.1016/j.conbuildmat.2016.05.144>.
- BSWA Tech, 2022. *BSWA Impedance Tube Solutions*. [online] Available at: <<http://www.bswa-tech.com/?p=580&a=view&r=30>> [Accessed 28 August 2022].
- Chaisaenrith, P., Taksakulvith, P. and Pavasupree, S., 2021. Effect of nano titanium dioxide in intumescent fireproof coating on thermal performance and char morphology. *Materials Today: Proceeding*, [e-journal] 47(12), pp.3462-3467. <https://doi.org/10.1016/j.matpr.2021.03.461>.

Chemical Book, 2017. *1318-00-9(VERMICULITE) Product Description*. [online] Available at:

<https://www.chemicalbook.com/ChemicalProductProperty_US_CB7312881.aspx> [Accessed 26 July 2022].

Cheng, J.J., Niu, S.S., Zhao, Y.Q., Liu, Y.Q., Kang, M.Y., Guan, Y. and Zhang, F., 2022. The flame retardant and thermal conductivity properties of high thermal conductivity expandable graphite microcapsule filled natural rubber composites. *Constructions and Building Materials*, [e-journal] 318. <https://doi.org/10.1016/j.conbuildmat.2021.125998>.

Clariant, 2016. *Safety Data Sheet*. [online] Available at: <<https://www.palmerholland.com/Assets/User/Documents/Product/42114/870/MITM02885.PDF>> [Accessed 18 August 2022].

Cui, M.J., Li, J., Qin, D.B., Sun, J.K., Chen, Y., Xiang, J. and Yan, J., 2021. Intumescent flame-retardant behaviour of triazine group and ammonium polyphosphate in waterborne polyurethane. *Polymer Degradation and Stability*, [e-journal] 183. <https://doi.org/10.1016/j.polymdegradstab.2020.109439>.

CWS, 2022. *Fire protection ducts*. [online] Available at: <<https://www.cws.com/en/fire-safety/fire-protection-ducts#:~:text=Fire%20protection%20ducts%20%28L-I-duct%20as%20well%20as%20E-duct%29,contribute%20to%20the%20protection%20of%20people%20and%20buildings.>>> [Accessed 30 June 2022].

Dokumen, 2023. *Supplementary User Manual for BSWA Impedance Tube Measurement Systems*. [online] Available at: <<https://dokumen.tips/documents/supplementary-user-manual-for-bswa-impedance-tube-user-manual-for-bswa-impedance.html?page=1>> [Accessed 7 April 2023].

Feng, J., Chen, Y., Liu, X.H., Liu, T.D., Zou, L.Y., Wang, Y.T., Ren, Y.M., Fan, Z.J., Lv, Y.Z. and Zhang, M.L., 2013. In-situ hydrothermal crystallization Mg(OH)₂ films on magnesium alloy AZ91 and their corrosion resistance properties. *Materials Chemistry and Physics*, [e-journal] 143(1), pp.322-329. <https://doi.org/10.1016/j.matchemphys.2013.09.005>.

Fire Trace, 2022. *Smoke extract and dual ventilation*. [online] Available at: <<http://www.firetrace-ductwork.co.uk/dual-ventilation.php>> [Accessed 28 June 2022].

Flame Retardants, 2022. *Melamine*. [online] Available at: <http://fr.polymerinsights.com/fr-types/nitrogen-based/melamine?fbclid=IwAR2bjr3xFFjF3r84tzt8XbTP7c5TfVT4c_8SfTWK_rTtShgCQsobx6duARrQ> [Accessed 3 August 2022].

Fredj, N., Cohendoz, S., Feaugas, X. and Touzain, S., 2008. Effect of mechanical stress on kinetics of degradation of marine coatings. *Progress in*

Organic Coatings, [e-journal] 63(3), pp.316-322.
<https://doi.org/10.1016/j.porgcoat.2008.05.001>.

Fu, S., Song, P. and Liu, X., 2017. 19 - Thermal and flame retardancy properties of thermoplastics/natural fiber biocomposites. *Advanced High Strength Natural Fibre Composites in Construction*, [e-journal] pp.479-508.
<https://doi.org/10.1016/B978-0-08-100411-1.00019-4>.

Han, X.W., Guo, S. and Pan, H.Y., 2022. Construction of Mg(OH)₂/graphene oxide nanostructures with advanced adsorbing and flame-retardancy performance. *Materials Chemistry and Physics*, [e-journal] 290.
<https://doi.org/10.1016/j.matchemphys.2022.126653>.

Jong, J.K.Y., Yew, M.C., Yew, M.K. and Saw, L.H., 2019. Preparation of intumescent fire protective coating for fire rated timber door. *Coatings*, [e-journal] 9(11), 738. <https://doi.org/10.3390/coatings9110738>.

Kakhia, T., 2023. *Antifoaming Agents* [online] Available at: <https://tarek.kakhia.org/books_eng/Defoamer.Tarek_Kakhia.pdf#:~:text=Generally%20a%20defoamer%20is%20insoluble%20in%20the%20foaming,the%20surface%20of%20the%20bulk%20liquid%20more%20quickly> [Accessed 11 March 2023].

Karlsson, L., Lundgren, A., Jungqvist, J and Hjertberg, T., 2009. Influence of melt behaviour on the flame-retardant properties of ethylene copolymers modified with calcium carbonate and silicone elastomer. *Polymer Degradation and Stability*, [e-journal] 94, pp.527-532.
<http://dx.doi.org/10.1016%2Fj.polyimdegradstab.2009.01.025>.

Karthik, J., Surendra, H.J., Prathiba, V.S. and Kumar, G.A., 2022. Experimental study on lightweight concrete using Leca, silica fume, and limestone as aggregates. *Materials Today: Proceedings*, [e-journal].
<https://doi.org/10.1016/j.matpr.2022.06.453>.

Koorsen Fire & Safety, 2020. *How does a fire alarm system work?* [online] Available at: <<https://blog.koorsen.com/how-does-a-fire-alarm-system-work>> [Accessed 30 June 2022].

Kubba, S., 2010. Chapter Six - Green Building Materials and Products. *LEED practices, certification, and accreditation handbook*, [e-journal] pp.151-209.
<https://doi.org/10.1016/B978-1-85617-691-0.00006-0>.

Li, M.L., Zhao, Y.L., Ai, Z., Bai, H.Y., Zhang, T.T. and Song S.X., 2021. Preparation and application of expanded and exfoliated vermiculite: A critical review. *Chemical Physics*, [e-journal] 550.
<https://doi.org/10.1016/j.chemphys.2021.111313>.

Li, R.L., Wang, N., Bai, Z.Y., Chen, S.P., Guo, J.B. and Chen, X.L., 2021. Microstructure design of polypropylene/expandable graphite flame retardant composites toughened by the polyolefin elastomer for enhancing its mechanical

properties. *RSC Advances*, [e-journal] 11. <https://doi.org/10.1039/D0RA09978C>.

Li, X., Shi, T.X., Chang, P., Hu, H., Xie, J.Y. and Liu, Y.Y., 2014. Preparation of magnesium hydroxide flame retardant from light calcined powder by ammonia circulation method. *Powder Technology*, [e-journal] 260(2014), pp.98-104. <https://doi.org/10.1016/j.powtec.2014.03.051>.

Liu, Y., Gao, Y.S., Zhang, Z. and Wang, Q., 2021. Preparation of ammonium polyphosphate and dye co-intercalated LDH/polypropylene composites with enhanced flame retardant and UV resistance properties. *Chemosphere*, [e-journal] 277. <https://doi.org/10.1016/j.chemosphere.2021.130370>.

Mallard Creek Polymers, 2021. *An introduction to vinyl acetate-based polymers*. [online] Available at: <[https://www.mcpolymers.com/library/vinyl-acetate-based-polymers#:~:text=reaction%20is%20shown..-,Vinyl%20acetate%20monomers%20\(VAM\)%20are%20essential%20building%20blocks%20for%20a,structure%20of%20vinyl%20acetate%20monomer](https://www.mcpolymers.com/library/vinyl-acetate-based-polymers#:~:text=reaction%20is%20shown..-,Vinyl%20acetate%20monomers%20(VAM)%20are%20essential%20building%20blocks%20for%20a,structure%20of%20vinyl%20acetate%20monomer)> [Accessed 27 July 2022].

Mei Wang Chemical, 2022. *Vinyl Resin Acrylic Copolymer Emulsion Vdar- (-21) for Fire Retardant Vinyl Resin*. [online] Available at: <<https://www.mwflameretardant.com/showroom/vinyl-resin-acrylic-copolymer-emulsion-vdar-21-for-fire-retardant-vinyl-resin.html>> [Accessed 18 March 2023].

Merck, 2020. *Safety Data Sheet*. [online] Available at: <<https://www.sigmaaldrich.com/MY/en/sds/sial/nistrm8988>> [Accessed 25 August 2022].

National Center for Biotechnology Information, 2022. *Calcium carbonate*. [online] Available at: <<https://pubchem.ncbi.nlm.nih.gov/compound/Calcium-carbonate>> [Accessed 16 August 2022].

National Center for Biotechnology Information, 2022. *Melamine*. [online] Available at: <<https://pubchem.ncbi.nlm.nih.gov/compound/melamine>> [Accessed 3 August 2022].

National Center for Biotechnology Information, 2022. *Pentaerythritol*. [online] Available at: <<https://pubchem.ncbi.nlm.nih.gov/compound/Pentaerythritol>> [Accessed 3 August 2022].

Nguyen, G.T., Ly, T.N., Tran, N.T., Tuan, H.N.A, Hieu, N.H. and Bui, T.H., 2023. Glutaric acid/expanded graphite composites as highly efficient shape-stabilized phase change materials at medium-temperature. *Journal of Energy Storage*, [e-journal] 63. <https://doi.org/10.1016/j.est.2023.107038>.

OBO Bettermann, 2022. *PYROLINE® Con S I90/E30 protection duct*. [online] Available at: <<https://www.obo.global/products/safety-and-protection-installations/fire-protection-ducts-protection-of-escape-routes/pyroline-con-s>>

[concrete-fire-protection-duct/pyroline-con-s/fire-protection-duct-i90-e30.html](https://doi.org/10.1016/j.carbpol.2021.118108)> [Accessed 30 June 2022].

Oliveira, C.R.S., Batistella, M.A., Souza, S.M.A.G.U. and Souza, A.A.U., 2021. Functionalization of cellulosic fibers with a kaolinite-TiO₂ nano-hybrid composite via a solvothermal process for flame retardant applications. *Carbohydrate Polymers*, [e-journal] 266(2021). <https://doi.org/10.1016/j.carbpol.2021.118108>.

Orhan, T., Isitman, N.A., Hacaloglu, J. and Kaynak, C., 2011. Thermal degradation mechanisms of aluminium phosphinate, melamine polyphosphate and zinc borate in poly(methyl methacrylate). *Polymer Degradation and Stability*, [e-journal] 96(10), pp.1780-1787. <https://doi.org/10.1016/j.polymdegradstab.2011.07.019>.

Panel Built Incorporated, 2022. *Fire rated wall panels | Fire resistant wall panels*. [online] Available at: <<https://www.panelbuilt.com/products/fire-rated-wall-panels>> [Accessed 28 June 2022].

Park, S.S., Lee, J.S., Yoon, K.B., Woo, S.W. and Lee, D.E., 2021. Application of an Acrylic Polymer and Epoxy Emulsion to Red Clay and Sand. *Polymers (Basel)*, [e-journal] 13(19). <https://doi.org/10.3390/polym13193410>.

Pondelak, A., Skapin, A.S., Knez, N., Knez, F. and Pazlar, T., 2021. Improving the flame retardancy of wood using an eco-friendly mineralisation process. *Green Chemistry*, [e-journal] 23, pp.1130-1135. <https://doi.org/10.1039/D0GC03852K>.

Poon, C.K. and Kan, C.W., 2015. Effects of TiO₂ and curing temperatures on flame retardant finishing of cotton. *Carbohydrate Polymers*, [e-journal] 121, pp.457-467. <https://doi.org/10.1016/j.carbpol.2014.11.064>.

Promat, 2019. *Fire protective boards – Constructing safer buildings*. [online] Available at: <<https://www.promat.com/en-my/construction/projects/expert-area/39617/fire-protective-boards/>> [Accessed 28 June 2022].

Promat, 2022. *Passive fire protection with calcium silicate materials*. [online] Available at: <<https://www.promat.com/en/industry/technologies/calcium-silicates/passive-fire-protection/>> [Accessed 29 June 2022].

Rabello, L.G. and Ribeiro, R.C.C., 2021. A novel vermiculite/ vegetable polyurethane resin-composite for thermal insulation eco-brick production. *Composites Part B*, [e-journal] 221. <https://doi.org/10.1016/j.compositesb.2021.109035>.

Rise Home Design Inc., 2023. *Sheathing > Magnesium Oxide Board: Learn About This Product*. [online] Available at: <<https://www.buildwithrise.com/products/building-envelope-and-structure/wall-assemblies/sheathing/magnesium-oxide-board>> [Accessed 22 April 2023].

Riyazuddin, Rao, T.N., Huassain, T. and Koo, B.H., 2020. Effect of aluminum tri-hydroxide/zinc borate and aluminium tri-hydroxide/melamine flame retardant systems synergies on epoxy resin. *Materials Today: Proceedings*, [e-journal] 27(3), pp.2269-2272. <https://doi.org/10.1016/j.matpr.2019.09.110>.

Rode, C., Nielsen, T.B., Hansen, K.K. and Grell, B., 2017. Moisture damage with magnesium oxide boards in Danish facade structures. *Energy Procedia*, [e-journal] 132, pp.765-770. <https://doi.org/10.1016/j.egypro.2017.10.025>.

Santos, P. S., Santos, H.S. and Toledo, S.P., 2000. Standard Transition Aluminas. Electron Microscopy Studies. *Materials Research*, [e-journal] 3(4), pp.104-114. <https://doi.org/10.1590/S1516-14392000000400003>.

Sigma-Aldrich, 2020. *Safety Data Sheet*. [online] Available at: <<https://www.sigmaaldrich.com/MY/en/sds/sigald/239216>> [Accessed 25 August 2022].

Sigma-Aldrich, 2021. *Safety Data Sheet*. [online] Available at: <<https://www.sigmaaldrich.com/MY/en/sds/aldrich/742503>> [Accessed 18 August 2022].

Sigma-Aldrich, 2021. *Safety Data Sheet*. [online] Available at: <<https://www.sigmaaldrich.com/MY/en/sds/aldrich/m265>> [Accessed 18 August 2022].

Sigma-Aldrich, 2021. *Safety Data Sheet*. [online] Available at: <<https://www.sigmaaldrich.com/MY/en/sds/sigald/11028>> [Accessed 18 August 2022].

Sigma-Aldrich, 2022. *Safety Data Sheet*. [online] Available at: <<https://www.sigmaaldrich.com/MY/en/sds/sigald/310093>> [Accessed 25 August 2022].

Sigma-Aldrich, 2023. *Safety Data Sheet*. [online] Available at: <<https://www.sigmaaldrich.com/MY/en/sds/aldrich/282863>> [Accessed 18 March 2023].

Sun, Q., Ding, Y., Stoliarov, S.I., Sun, J.H., Fontaine, G. and Bourbigot, S., 2020. Development of a pyrolysis model for an intumescent flame retardant system: Poly(lactic acid) blended with melamine and ammonium polyphosphate. *Composites Part B*, [e-journal] 194. <https://doi.org/10.1016/j.compositesb.2020.108055>.

Sunrock, 2022. *Fire resistant boards for buildings & walls*. [online] Available at: <[Fire Resistant Boards for Building and Walls | Thermocare India](#)> [Accessed 28 June 2022].

Taylor, J., 2020. *What are the advantages and disadvantages of gypsum board?* [online] Available at: <<https://gharpedia.com/blog/advantages-and-disadvantages-gypsum-board/>> [Accessed 7 July 2022].

The Vermiculite Association, 2022. *Properties*. [online] Available at <<https://www.vermiculite.org/resources/properties>> [Accessed 26 July 2022].

Thirumal, M., Khastgir, D., Nando, G.B., Naik, Y.P. and Singha, N.K., 2010. Halogen-free flame retardant PUF: Effect of melamine compounds on mechanical, thermal and flame retardant properties. *Polymer Degradation and Stability*, [e-journal] 95(6), pp.1138-1145. <https://doi.org/10.1016/j.polymdegradstab.2010.01.035>.

Tomiak, F., Rathberger, K., Schoffel, A. and Drummer, D., 2021. Expandable Graphite for Flame Retardant PA6 Applications. *Fire and Polymers*, [e-journal] 13(16). <https://doi.org/10.3390/polym13162733>.

Toro, P., Quijada, R., Pedram, M.Y. and Arias, J.L., 2007. Eggshell, a new bio-filler for polypropylene composites. *Materials Letters*, [e-journal] 61(22), pp.4347-4350. <https://doi.org/10.1016/j.matlet.2007.01.102>.

Wang, G.J. and Yang, J.Y., 2010. Influences of binder on fire protection and anticorrosion properties of intumescent fire resistive coating for steel structure. *Surface and Coatings Technology*, [e-journal] 24(8), pp.1186-1192. <https://doi.org/10.1016/j.surfcoat.2009.10.040>.

Wang, G.J. and Yang, J.Y., 2012. Influences of molecular weight of epoxy binder on fire protection of waterborne intumescent fire resistive coating. *Surface & Coatings Technology*, [e-journal] 206 (8-9), pp.2146-2151. <https://doi.org/10.1016/j.surfcoat.2011.09.050>.

Wang, W., Peng, Y., Zhang, W. and Li, J.Z., 2015. Effect of pentaerythritol on the properties of wood- flour/polypropylene/ammonium polyphosphate composite system. *BioRes*, [online] Available at: <<https://bioresources.cnr.ncsu.edu/resources/effect-of-pentaerythritol-on-the-properties-of-wood-flourpolypropyleneammonium-polyphosphate-composite-system/>> [Accessed 3 August 2022].

Wang, W., Wen, P.Y., Zhan, J., Hong, N.N., Cai, W., Gui, Z. and Hu, Y., 2017. Synthesis of a novel charring agent containing pentaerythritol and triazine structure and its intumescent flame retardant performance for polypropylene. *Polymer Degradation and Stability*, [e-journal] 144, pp.454-463. <http://dx.doi.org/10.1016/j.polymdegradstab.2017.09.011>.

Wang, Z.Y., Han, E.H. and Ke, W., 2006. Influence of expandable graphite on fire resistance and water resistance of flame-retardant coatings. *Corrosion Science*, [e-journal] 49, pp.2237-2253. <https://doi.org/10.1016/j.corsci.2006.10.024>.

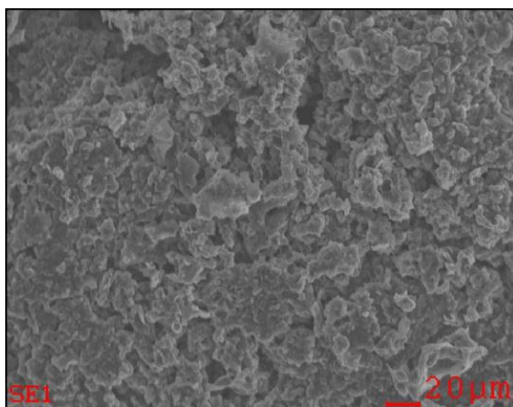
- Xu, Q.F., Chen, L.Z., Harries, K.A., Zhang, F.W., Liu, Q. and Feng, J.H., 2015. Combustion and charring properties of five common constructional wood species from cone calorimeter tests. *Construction and Building Materials*, [e-journal] 96, pp.416-427. <https://doi.org/10.1016/j.conbuildmat.2015.08.062>.
- Xu, Q.F., Wang, Y., Chen, L.Z., Gao, R.D. and Li, X.M., 2016. Comparative experimental study of fire-resistance ratings of timber assemblies with different fire protection measures. *Advances in Structural Engineering*. [e-journal] 19(3). <https://doi.org/10.1177/1369433216630044>.
- Xu, W.Z., Wang, G.S., Xu, J.Y., Liu, Y.C., Chen, R. and Yan, H.Y., 2019. Modification of diatomite with melamine coated zeolitic imidazolate framework-8 as an effective flame retardant to enhance flame retardancy and smoke suppression of rigid polyurethane foam. *Journal of Hazardous Materials*, [e-journal] 379. <https://doi.org/10.1016/j.jhazmat.2019.120819>.
- Xu, S.Y., Han, Y., Zhou, C., Li, J.X., Shen, L.G. and Lin, H.J., 2022. A biobased flame retardant towards improvement of flame retardancy and mechanical property of ethylene vinyl acetate. *Chinese Chemical Letters*, [e-journal]. <https://doi.org/10.1016/j.ccllet.2022.02.008>.
- Xu, T., Huang, X.M. and Zhao, Y.L., 2011. Investigation into the properties of asphalt mixtures containing magnesium hydroxide flame retardant. *Fire Safety Journal*, [e-journal] 46(2011), pp.330-334. <https://doi.org/10.1016/j.firesaf.2011.05.001>.
- Xu, Z.S., Chu, Z.Y., Yan, L. and Chen, H.G., 2018. Effect of chicken eggshell on the flame-retardant and smoke suppression properties of an epoxy-based traditional APP-PER-MEL system. *Polymer Composites*, [e-journal] 40(7), pp.2712-2723. <https://doi.org/10.1002/pc.25077>.
- Yew, M.C. and Sulong, N.H.R., 2012. Fire-resistive performance of intumescent flame-retardant coatings for steel. *Materials and Design*, [e-journal] 34, pp.719-724. <https://doi.org/10.1016/j.matdes.2011.05.032>.
- Yew, M.C., Sulong, N.H.R., Yew, M.K., Amalina, M.A. and Johan, M.R., 2014. Fire propagation performance of intumescent fire protective coatings using eggshells as a novel biofiller. *Scientific World Journal*, [e-journal] 2014. <https://doi.org/10.1155/2014/805094>.
- Yew, M.C., Yew, M.K., Saw, L.H., Ng, T.C., Duraijar, R. and Beh, J.H., 2018. Influences of nano bio-filler on the fire-resistive and mechanical properties of water-based intumescent coatings. *Progress in Organic Coatings*, [e-journal] 124, pp.33-40. <https://doi.org/10.1016/j.porgcoat.2018.07.022>.
- Yin, Z.T., Lu, J.Y., Yu, X.L., Jia, P.F., Tang, G., Zhou, X.D., Lu, T.T., Guo, L.Y., Wang, B.B., Song, L. and Hu, Y., 2021. Construction of a core-shell structure compound: Ammonium polyphosphate wrapped by rare earth compound to achieve superior smoke and toxic gases suppression for flame

retardant flexible polyurethane foam composites. *Composites Communications*, [e-journal] 28. <https://doi.org/10.1016/j.coco.2021.100939>.

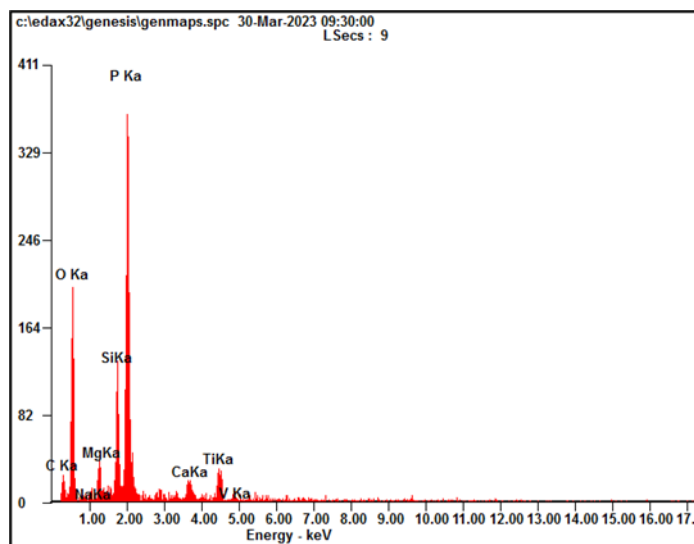
Zhang, H.Y., Wang, H.Q. and Wang, H.Q., 2018. Flame retardant mechanism and surface modification of magnesium hydroxide flame retardant. *Earth and Environmental Science*, [online] Available at: <<https://iopscience.iop.org/article/10.1088/1755-1315/170/3/032028/pdf>> [Accessed 21 July 2022].

APPENDICES

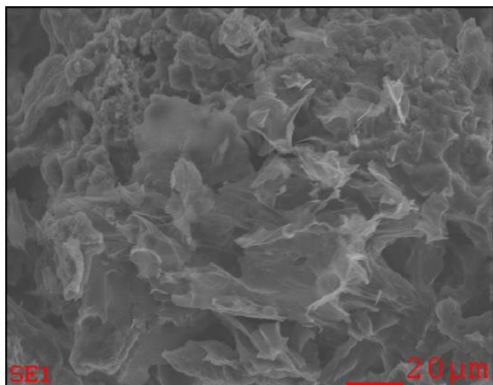
Appendix A: Graphs



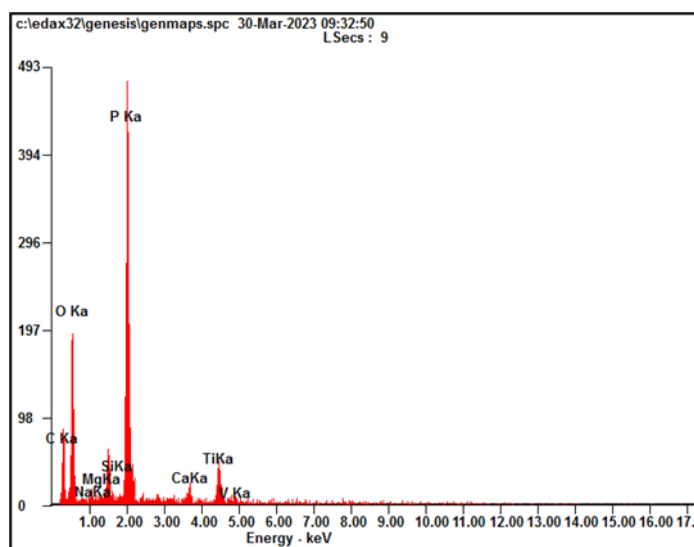
<i>Element</i>	<i>Wt%</i>	<i>At%</i>
<i>CK</i>	12.94	21.32
<i>OK</i>	39.47	48.81
<i>NaK</i>	00.55	00.48
<i>MgK</i>	02.88	02.35
<i>SiK</i>	07.99	05.63
<i>PK</i>	27.87	17.81
<i>CaK</i>	02.40	01.19
<i>TiK</i>	05.54	02.29
<i>VK</i>	00.35	00.14
<i>Matrix</i>	Correction	ZAF



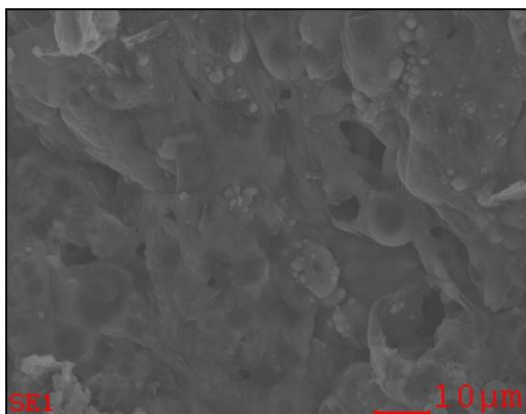
Appendix A-1: EDX result for sample S1.



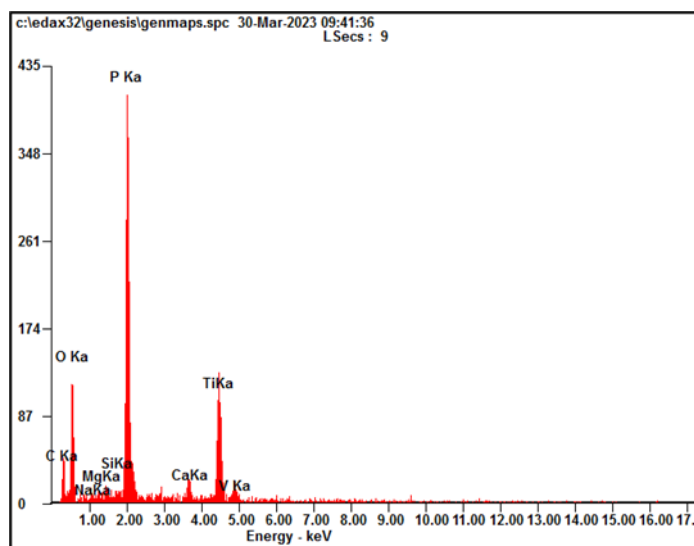
<i>Element</i>	<i>Wt%</i>	<i>At%</i>
<i>CK</i>	27.61	40.52
<i>OK</i>	37.19	40.97
<i>NaK</i>	00.42	00.32
<i>MgK</i>	00.18	00.13
<i>SiK</i>	00.24	00.15
<i>PK</i>	25.59	14.56
<i>CaK</i>	01.71	00.75
<i>TiK</i>	06.52	02.40
<i>VK</i>	00.55	00.19
<i>Matrix</i>	Correction	ZAF



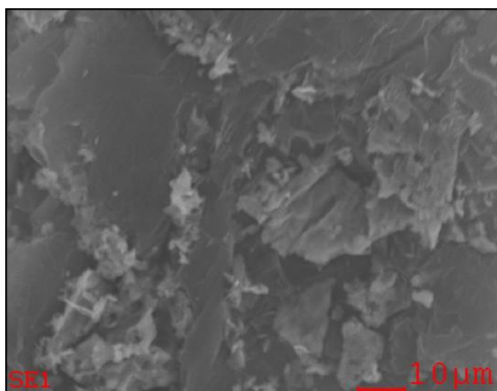
Appendix A-2: EDX result for sample S2.



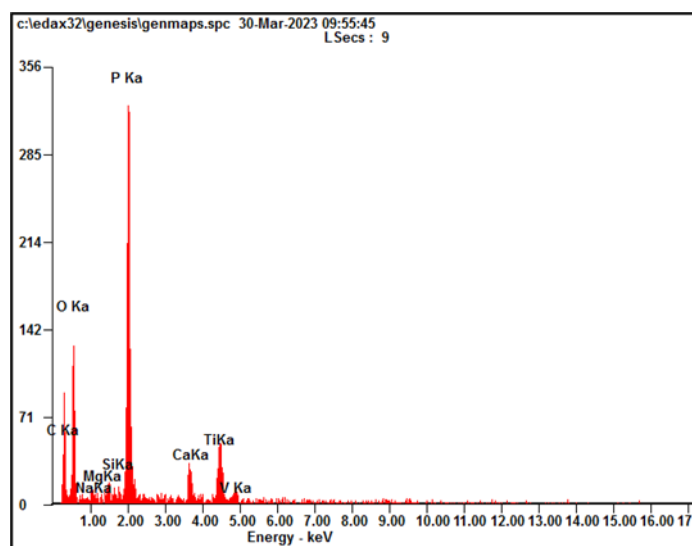
<i>Element</i>	<i>Wt%</i>	<i>At%</i>
<i>CK</i>	17.17	29.48
<i>OK</i>	32.30	41.62
<i>NaK</i>	00.52	00.47
<i>MgK</i>	00.32	00.27
<i>SiK</i>	00.61	00.45
<i>PK</i>	27.27	18.16
<i>CaK</i>	02.25	01.16
<i>TiK</i>	18.95	08.16
<i>VK</i>	00.61	00.25
<i>Matrix</i>	Correction	ZAF



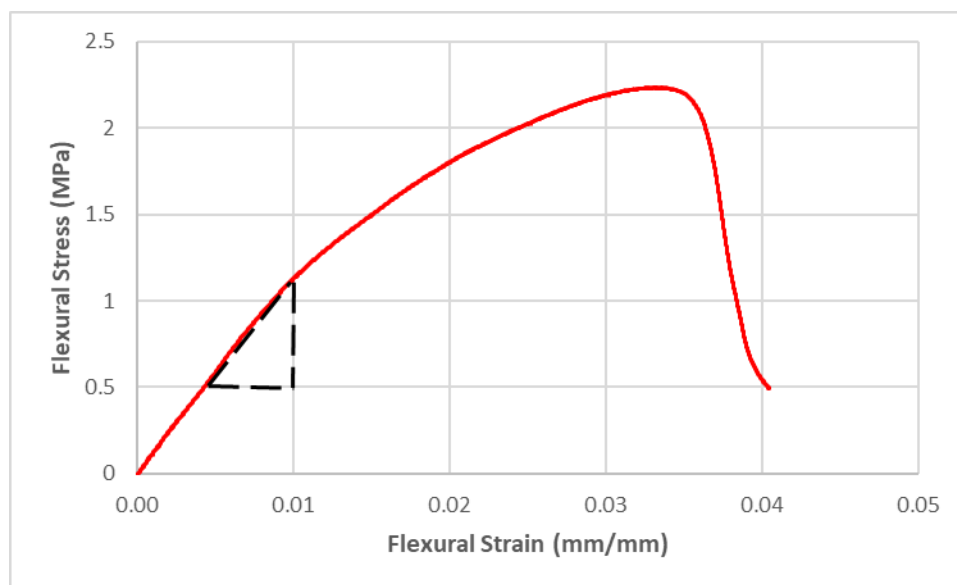
Appendix A-3: EDX result for sample S3.



<i>Element</i>	<i>Wt%</i>	<i>At%</i>
<i>CK</i>	27.69	41.68
<i>OK</i>	33.95	38.37
<i>NaK</i>	00.69	00.54
<i>MgK</i>	00.28	00.21
<i>SiK</i>	00.50	00.32
<i>PK</i>	22.76	13.28
<i>CaK</i>	03.61	01.63
<i>TiK</i>	10.15	03.83
<i>VK</i>	00.36	00.13
<i>Matrix</i>	Correction	ZAF



Appendix A-4: EDX result for sample S4.



Appendix A-5: Sample calculation of Flexural Stress and Flexural Modulus.

Taking P4 as the sample calculation:

L = span length (mm)	= 150 mm
b = width of test sample (mm)	= 30 mm
d = depth or thickness of test sample (mm)	= 40 mm
F = load at a given point on the load deflection curve (N)	= 476 N
m = gradient or slope of the initial straight line of the load deflection curve (N/mm)	= $\left(\frac{1.1828-0.5737}{0.01-0.005}\right)$
	= 121.86 N/mm

Flexural Stress, σ_f







$$\begin{aligned}\sigma_f &= \frac{3FL}{2bd^2} \\ &= \frac{3(476)(150)}{2(30)(40)^2} \\ &= 2.2313 \text{ MPa}\end{aligned}$$

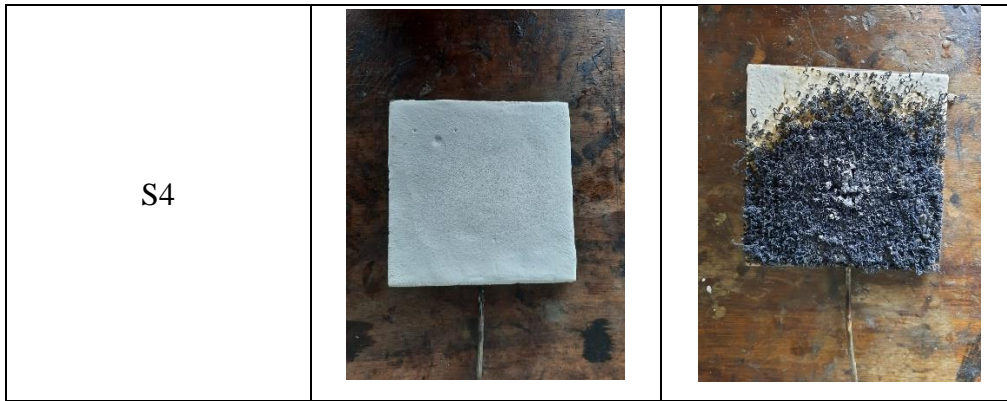
Flexural Modulus, E_f

$$\begin{aligned}E_f &= \frac{L^3 m}{4bd^3} \\ &= \frac{(150^3)(121.86)}{4(30)(40)^3} \\ &= 53.55 \text{ N/mm}^2\end{aligned}$$

Appendix B: Tables

Appendix B-1: The difference between samples before and after the Bunsen burner test.

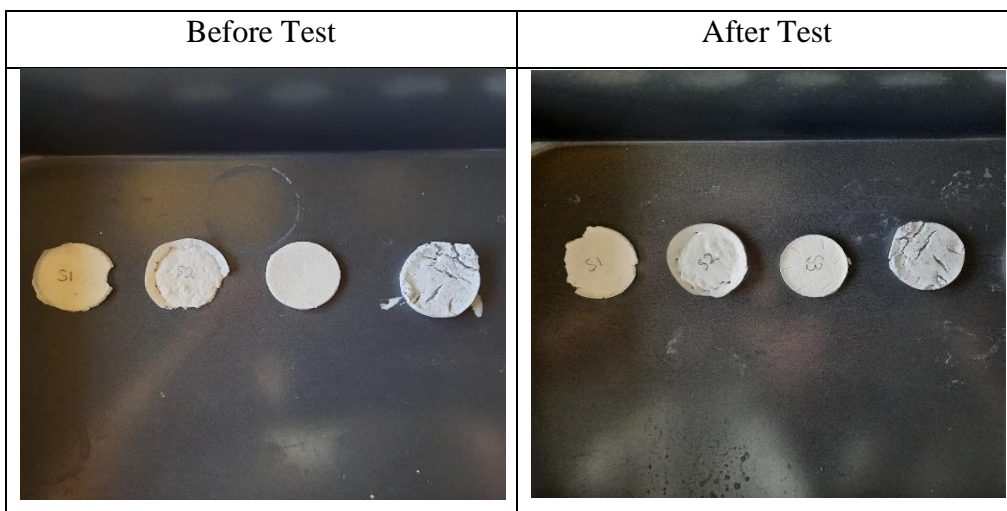
Samples	Before Test	After test
S1		
S2		
S3		









Appendix B-2: The sample weight before and after the static immersion test.

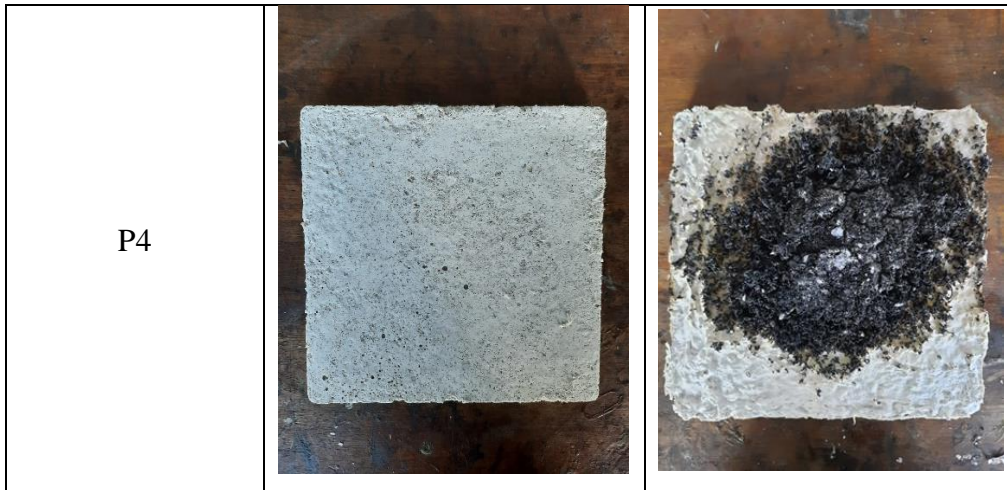
Samples	Average Weight (g)				
	Initial weight (W_0)	1 st Day	2 nd Day	3 rd Day	4 th Day
S1	0.6725	1.6785	1.0402	1.0100	0.9894
S2	0.8100	1.1371	1.0817	1.0455	1.0072
S3	1.0220	1.2665	1.2801	1.2570	1.2380
S4	3.011	3.9942	3.9191	3.725	3.6052

Appendix B-3: The difference between samples before and after the Static Immersion test.

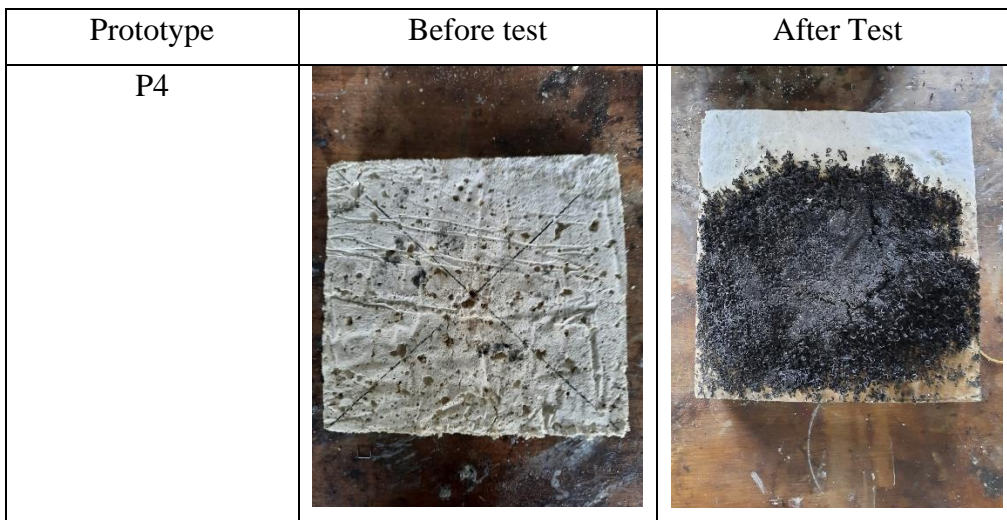


Appendix B-4: The difference of prototypes before and after carrying out the Half-hour Small-scale Fire test.

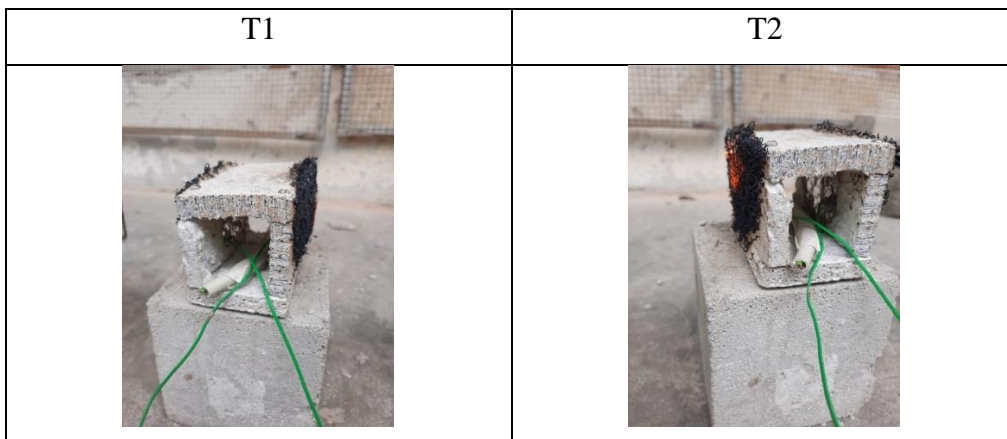
Prototypes	Before Test	After test
P1	 A square, light-colored, porous material sample, likely a prototype, shown before the fire test. It has a uniform, slightly textured appearance.	 The same square sample after a half-hour fire test. The top surface is heavily charred and blackened, with a distinct white, crystalline residue in the center. The bottom edge shows a clear boundary between the charred top and the unburned bottom.
P2	 A square, light-colored, porous material sample, similar to P1, shown before the fire test.	 The same square sample after a half-hour fire test. The top surface is heavily charred and blackened, with a distinct white, crystalline residue in the center. The bottom edge shows a clear boundary between the charred top and the unburned bottom.
P3	 A square, light-colored, porous material sample, similar to P1 and P2, shown before the fire test.	 The same square sample after a half-hour fire test. The top surface is heavily charred and blackened, with a distinct white, crystalline residue in the center. The bottom edge shows a clear boundary between the charred top and the unburned bottom.



Appendix B-5: The difference of prototype P4 before and after the 1-hour Small-scale Fire test.



Appendix B-6: Char layers formed at both side of the Fire Protection duct to protect the Electrical cable.



Appendix C: Project Outcomes



Appendix C-1: Silver Award is Obtained in Final Year Project Poster Competition with Certificate and Cash prize of RM 120.

Recent Development of Lightweight Fire-rated Board for the Safety-Relevant Circuits

You Yi Lim¹ and Ming Chian Yew¹

¹ Department of Mechanical and Material Engineering, Lee Kong Chian Faculty of Engineering and Science, Universiti Teknologi Abdul Rahman, Cheras 43000 Kajang, Malaysia; e-mail: yewmctutar.edu.my

* Correspondence: yewmctutar.edu.my ; yewmingchian@gmail.com; Tel.: +60390860288

Abstract

Fire protection ducts store and protect electrical cables during a fire outbreak. The cables provide power supplies to the active fire protective system (e.g., water sprinklers, fire alarms) and extend the time for evacuation. Fire protection duct can be fabricated by combining and assembling fire-retardant boards. Non-halogenated fire-retardant materials yield sufficient protective barriers for the passive fire protection system (e.g., fire-rated timber doors, smoke dampers). Thus, the project scope focuses on formulating the water-based intumescent binder (W-IB) as the fundamental of the fire-retardant board. In the analysis, four groups of W-IB were formulated and analysed through fire resistance testing (e.g., Bunsen burner test), chemical testing (e.g., static immersion test), mechanical testing (e.g., adhesion strength test), thermal testing (e.g., TGA test), and physical testing (e.g., SEM/EDX test, FTIR test). Next, W-IB and vermiculite were combined to make fire-retardant board prototypes. To ascertain the compositions' best performance, a half-hour small-scale fire, a density measurement, a sound insulation, and a three-point flexural tests were conducted. The leading-performing fire-retardant board was then cast using the best-performing compositions. The capabilities of the fire-retardant board and the commercial Magnesium Oxide (MgO) board were compared using a 1-hour small-scale fire test and density measurement test. The leading-performing fire-retardant board was then used to construct a small-scale fire protection duct. The results of all the tests revealed that, both pre and post of the 1-hour small-scale fire test, fire-retardant board prototype 4 (P4) has a lower weight loss percentage than commercial MgO board. Prototype P4 has a weight loss of 20.6 % lower than commercial MgO board. Thus, prototype P4 has better suitability to construct fire protection duct. On the other hand, prototype P4 also showed a lower temperature profile (100 °C) than the commercial MgO board (220 °C) when conducting the 1-hour small-scale fire test. Therefore, prototype P4 possesses an effective W-

IB that can resist the fire propagation and remain its technical integrity after a 1-hour small-scale fire test.

Keywords: Fire protection; Fire rated board; Flame-retardant; Intumescent

1. Introduction

Human lifestyles have started to change due to the convenience made by modern technologies. As an example, employees have changed their working environment from outdoor to indoor offices. Instead of working under the natural sunlight, people nowadays spend most of their time in the indoor environment.

In response to human behaviour changes, it is important to understand the purpose of fire protection systems in indoor buildings. When talking about the structure of a building, fire safety always comes to mind. It is essential for businesspeople as fire has an instantaneous response to spread in seconds. Business capital investment in fire protection systems brings a noteworthy benefit as they can reduce damage to the building structure, valuable equipment, important documents, etc.

The basic functions of fire protection systems are to reduce the fire spread rate and increase the human escape time. The common fire-protective appliances are the smoke detector and sprinkler. When the smoke detector detects the fire smoke, the sprinkler will be activated to release the water. Clean agents will replace the water during crucial moments.

A fire protection system can be classified into active and passive. An active fire protection system is a system whereby an action (automatic or manual) will be performed to extinguish a fire. It can be automatic, such as the sprinkler releasing the water when the temperature rises, whereas a fire extinguisher is an example of a manual method to reserve the escaping time and reduce the property's damage. Besides, passive fire protection systems are equally essential in fire safety as they are the structure of the building that resists fire spread. Examples include fire-resistant doors, smoke dampers, firewalls, etc. One of the influential factors that determine fire protection performance is the construction materials. For example, a fire-rated door has a good layer of thermal protection because it has flame-retardant additives, fillers, and a binder.

Appendix C-2: Draft of a Conference Paper to be Submitted in the local Conference.